Radiative 3D Powell Eyring Nanofluid Flow with Darcy-Forchheimer Effect past a nonlinear stretched surface

Thesis Submitted By

NAZIA SHAHMIR (01-248172-007)

Supervised By

Prof. Dr. M. Ramzan

A dissertation submitted to the Department of Computer Science, Bahria University, Islamabad as a partial fulfillment of the requirements for the award of the degree of MS

Session (2017 - 2019)

Bahria University
Discovering Knowledge

MS-13

Thesis Completion Certificate

Student's Name: **Nazia Shahmir** Registration No. **01-248172-007**
Program of Study: **MS(Mathematics)**
Thesis Title: **"Radiative 3-D Powell Eyring Nano fluid Flow with Darcy-Forchheimer Effect past a Nonlinear Stretched Surface"**

It is to certify that the above student's thesis has been completed to my satisfaction and, to my belief, its standard is appropriate for submission for Evaluation. I have also conducted plagiarism test of this thesis using HEC prescribed software and found similarity index at **14%** that is within the permissible limit set by the HEC for the MS/MPhil degree thesis. I have also found the thesis in a format recognized by the BU for the MS/MPhil thesis.

Principal Supervisor's Signature: _____ 21/06/2019

Date: **21-06-2019** Name: **Prof. Dr. M. Ramzan**

Dedicated to

My worthy parents and respected teachers whose prayers and support have always been a source of inspiration and encouragement for me.

Acknowledgments

I am thankful to Almighty ALLAH Who has enabled me to learn and to achieve milestones towards my destination and His beloved Prophet Hazrat Muhammad (ﷺ) Who is forever a constant source of guidance, a source of knowledge and blessing for entire creation. His teachings show us a way to live with dignity, stand with honor and learn to be humble.

My acknowledgment is to my kind, diligent and highly zealous supervisor, Prof. Dr. M. Ramzan, who supported me with his cherished opinions and inspirational discussions. His valuable expertise, comments, suggestions and instructions are most welcome that greatly improved the clarity of this document. I am placing my earnest thanks to Prof. Dr. M. Ramzan. I am so grateful to work under the supervision of such a great person.

My gratitude is to my honorable professors who took me to the apex of my academia with their guidance. In particular, Prof. Dr. Rizwan and Dr. Jafar Hasnain who have always been supportive in all of my course work and kept encouraging me throughout the session in Bahria University, Islamabad Campus. They are the true teachers who have made Mathematics Department of BUIC, a real place of learning.

My intense recognition is to my father, mother, brothers, sisters and Hina Gull (for everything) who are always real pillars for my encouragement and showered their everlasting love, care and support throughout my life. Humble prayers, continuing support and encouragement of my family are as always highly appreciated. Consequently, My all plea is to Allah, the Almighty, the beneficent Whose blessings are always showered upon me via strengthening my wis- dom and bestowed me with the knowledge of what he wants.

Nazia Shahmir

Bahria University Islamabad, Pakistan May 2019

Abstract

A mathematical model is envisaged to scrutinize the Darcy Forchheimer flow of 3D Eyring Powell nanofluid flow in a porous media. The flow is subjected to zero mass flux and convective heat conditions at the boundary. The heat and mass transfer phenomena are analyzed in attendance of nonlinear thermal radiation and chemical reaction respectively. Apposite transformations are espoused to attain the system of highly nonlinear coupled differential equations and then undertaken by the Homotopy Analysis Method (HAM) to obtain the series solution. The physiognomies of numerous parameters versus the velocity, heat and mass transfer are depicted via graphs and cogitated accordingly. It is witnessed that for higher estimates of Schmidt number feeble concentration is observed. Furthermore the velocity of the fluid has declined for larger values of porosity number. The results obtained in the analysis are substantiated by erecting a comparative table with an established result in the literature. An outstanding matching is achieved in this regard.

Bahria University
Discovering Knowledge

MS-14A

Author's Declaration

I, **Nazia Shahmir** hereby state that my MS thesis titled **"Radiative 3-D Powell Eyring Nano fluid Flow with Darcy-Forchheimer Effect past a nonlinear stretched surface"** is my own work and has not been submitted previously by me for taking any degree from this university **Bahria University Islamabad**
or anywhere else in the country/world.

At any time if my statement is found to be incorrect even after my Graduate the university has the right to withdraw/cancel my MS degree.

Name of scholar: **Nazia Shahmir**
Date: **21/06/2019**

Bahria University
Discovering Knowledge

MS-14B

Plagiarism Undertaking

I solemnly declare that research work presented in the thesis titled **"Radiative 3-D Powell Eyring Nano fluid Flow with Darcy-Forchheimer Effect past a nonlinear stretched surface "** is solely my research work with no significant contribution from any other person. Small contribution / help wherever taken has been duly acknowledged and that complete thesis has been written by me.

I understand the zero tolerance policy of the HEC and Bahria University towards plagiarism. Therefore I as an Author of the above titled thesis declare that no portion of my thesis has been plagiarized and any material used as reference is properly referred / cited.

I undertake that if I am found guilty of any formal plagiarism in the above titled thesis even after award of MS degree, the university reserves the right to withdraw / revoke my MS degree and that HEC and the University has the right to publish my name on the HEC / University website on which names of students are placed who submitted plagiarized thesis.

Student / Author's Sign: _____

Name of the Student: **Nazia Shahmir**

LIST OF TABLES

LIST OF FIGURES

NOMENCLATURE

x, y, z	Coordinate axis
a, b	Dimensional constant
T_∞	Ambient fluid temperature
μ	Dynamic viscosity
η	Apparent viscosity
β, d_1	Fluid parameters
s	Consistency index
K	Mean absorption coefficient
n	Power law index
U_w, V_w	Surface stretching velocities
k	Thermal conductivity
u, v, w	Velocity components
ε, δ	Fluid parameters
We	Williamson parameter
α	Ratio parameter
A	Area
τ_w	Wall shear stress
Γ	Material constant
ν	Kinematic viscosity
ρ_f	Density of base fluid
$\frac{D}{D_t}$	Material time derivative
C_∞	Ambient fluid concentration
k^*	Permeability of spongy medium
β^*	non-Darcian coefficient
θ_f	Temperature ratio parameter
$\mathrm{Re}_x, \mathrm{Re}_y$	Local Reynolds numbers
F	Non- uniform inertial coefficient
C_b	Drag coefficient
T	Temperature
α^*	Thermal diffusivity

τ_{yx}	Shear force
D_T	Thermophoretic diffusion coefficient
τ	Stress Tensor
$\frac{dT}{dx}$	Temperature gradient
q	Heat flow
h	Convective heat transfer coefficient
k	Thermal conductivity
T_s	System temperature
e	Emissivity of the system
F_1	Force
τ^*	Stress tensor
δ_1	Chemical reaction parameter
$(\rho c)_f$	Heat capacity of fluid
h_f	Non-uniform heat transfer coefficient
T_f	Fluid reference Temperature
$(\rho c)_p$	Effective heat capacity of nanoparticles
C	Concentration
ρ	Density
p	Pressure
D_B	Brownian diffusivity
q_r	Radiative heat flux
k_c	Reaction rate
Ω	Nonlinear operator
ΔT	Temperature difference
T_w	Wall temperature
C_w	Wall's concentration
F_r	Forchheimer number
T_{ij}	Extra stress tensor
Pr	Prandtl number
I	Identity tensor
L	Characteristic length
Nb	Brownian motion parameter
d	Thickness of material
Nt	Thermophoresis parameter
σ^*	Stefan-Boltzmann
γ	Biot number
V	Volume

N	Newton
μ_0	Maximum viscosity
μ_∞	Minimum viscosity
k_1	Inertial permeability
b	Body force
Nu_x	Nusselt number
c_p	Specific heat capacity
ρ_f	Base fluid density
L^*	Strain tensor
c_f	Specific heat of base fluid
ρ_p	Density of nanoparticles
ψ	Stream function
λ	local porosity number
$\frac{du}{dx}$	Gradient of velocity
υ_f	Forchheimer velocity
Sc	Schmidt number
C_f	Skin friction

Contents

Chapter 1

Introduction and literature review

1.1 Introduction

Compared to solids, conventional heat transfer liquids innately have poor thermal conductivity. Emerging miniaturized technologies comparatively small channels would get blocked, if conventional liquids that contain mm or μm sized particles were to be used. Nanofluids (an advanced heat transfer coolant) are one of the latest developments of the nano technology. Nanofluids are highly efficient heat-transfer fluids prepared by dispersing nanoparticles less than 100 nm in diameter in conventional fluids. Anticipated increase was observed in the thermal conductivity as a result of the dispersion of nanoparticles in the base liquid. In many industrial fields like transportation, micro electronics, thermal therapy for cancer treatment etc, improved thermal behavior of nanofluids is of vital importance. Nanofluids have a remarkable combination of four characteristic properties intended in thermal and fluid systems:

- with low nanoparticle concentrations thermal conductivity is enhanced.
- strong temperature dependent thermal conductivity.
- nonlinear enhancement in thermal conductivity with (nanoparticle) concentration.
- rise in boiling critical heat flux.

Compared to base liquids, nanofluids are next generation heat transfer liquids because they provide exciting new posiibilities to improve heat transfer efficiency. In 1856, Henri Darcy(

a French civil engineer) in his publication put forward the quantitative theory of the flow of homogenous fluids through spongy media. He studied the flow characteristics of sand filters used to filter water in the city of France (Dijon). After these studies and experiments, he came forward with the results that "viscous forces dominate over inertial forces in porous media" which came to be known as Darcy Law, globally. Innate in the design of the Darcy flow model are the following characteristics:

- Darcy's law assumes laminar or viscous flow (creep velocity); inertia term (the fluid density) doesnot involve in it. This implies that the inertia forces in the liquid are being ignored which was not the case in classical Navier-Stokes equations.

- Darcy's law has this inherent supposition that in a poriferous media a vast surface area is subject to liquid's flow, as a result the viscosity will significantly surpass acceleration forces in the liquid unless turbulence is experienced.

With wide utilization in grain stockpiling, petroleum technology, frameworks of ground water and oil assests, this law is of immense importance in field of Fluid Mechanics. Places where the porous medium has larger flow rates due to non-uniformity, such as near the wall, Darcy law is not applicable there. Keeping this in mind one has to become mindful of the non-Darcian effect by porous medium in the flow analysis and heat transfer rate. A Dutch man named Philippe Forcchheimer, in 1901, while flowing gas thorough coal beds revealed that the relationship between flow rate and potential gradient is non-linear at comparatively greater velocity, and that non-linearity witnesses surge with increase in flow rate. He at the time was of view that the this non-linear increase was as a result of turbulence in the fluid flow (but it is now renowned that this non-linearity is due to inertial effects in the spongy media). However for increased flow rate, the mechanism of Forchheimer expression is deliberated. Basically, Forchheimer resulted in an improved relation called Darcy Forchheimer expression, by adding a quadratic term in motion equation. This term which is always there for a bigger Reynolds number was called as forcheimer term by Muskat in 1946. Physically, quadratic drag for spongy media in motion equation occurs for high filtration velocities, due to solid obstructs this drag is formed and becomes identical with drag at the surface by resistance. There are numerous examples of the possible situations of practical applications where the inertial effects can be

significant and darcy's law is no longer valid. For these situations, one may refer liquid flows in column reactors, in aquifers and in filters etc.

Recent enhancements in industrial applications have introduced a broad variety of non-newtonian liquids which are distinguished by various deviations from the viscous liquids. All those liquids for which the shear rate is changed and the shear stress doesn't change in the same proportion are considered to be non-newtonian. Hence, the difference of shear strength causes to alter the viscosity of these liquids, which is also called the "apparent viscosity" of the liquid. Richardson and Chhabra in 2018 defined the non-newtonian liquid, whose flow curve (shear stress against shear rate) is either nonlinear or that dont pass through the origin, which means that the apparent viscosity is not constant at a given pressure and temperature. These liquids are generally divided into three categories as time dependent, viscoelastic and time independent liquids. There have been numerous contributions from non-Newtonian liquids. Numerous things we use in our everyday life happen to be these kind of liquids. These are shampoo, toothpaste, sillyputty and whiped cream. It is renowned that mechanics of non-Newtonian liquids offer a certian challenge to mathematiciains and technologists. The nonlinearity may appear itself in numerous aspects in different fields such as biological-engineering and drilling operations. The Navier-Stokes approach is insufficient for such liquids and no single fundamental equation is provided in the literature which demonstrates the characteristics of all fluids. Thus, saveral non-Newtonian fluid models have been introduced. In which one of the model is prepared for chemical engineering systems is the Powell-Eyring fluid model.This rheological model has particular advantages over the other non-Newtonian formulations, including simplicity, ease of calculations and compactness.

1.2 Literature Review

Nanofluids, an emerging field of engineering has trapped the eye of numerous researchers who were looking at the ways to improve the efficiency of cooling processes in industry. This amalgamated fluid is unique in its own nature as nanofluids are prepared by inserting nanoparticles into the base fluids. By doing so, significant developement in the thermal conductivity of the base fluid is witnessed and the reason behind this fact is that solid metals have a higher ther-

mal conductivity in comparison to the base fluids. The verity was firstly revealed by Choi and Eastman [1] in 1995 who presented the idea that thermal conductivity is improved substantially once metallic nanosized (<100nm) are merged into the base fluids. This initiative has benefitted numerous engineering applications like transportation, chilling of microelectronic gadgets, and food processing processes [2-3]. The excellent features of nanoparticles like the infinitesimal size and small volume fraction make them highly adequate for preparation of nanofluids. The nanofluids under the influence of magnetohydrodynamics have also numerous interesting and practical applications like optical switches and modulators, drug delivery, optical fiber, and cancer therapy. Various studies have been conducted to reveal the different aspects of the nanofluid [4-15].

The material with stomata is termed as porous medium and is customarily filled by some liquid. A good number of applications including oil production, water flow in reservoirs and catalytic vessels etc. The idea of the flow of a liquid past a permeable media was first given by a French, Henry Darcy, in 1856 [16]. But this notion couldn't be so popular owing to its limitations of smaller porosity and low velocity. Subsequently, Philippes Forchheimer [17] modify the momentum equation with the addition of the square velocity term into the Darcian velocity to address the obvious deficiency. This term was later named by Muskat [18] as "Forchheimer term" which is true for high Reynolds number. Mondal and Pal [19] deliberated the Darcy-Forchheimer model over porous media past the linearly extended surface and concluded that concentration distribution is a diminishing function of electric field parameter. The flow of a hydromagnetic nanofluid past a Darcy-Forchheimer porous media with the impact of second-order boundary condition is examined numerically by Ganesh et al. [20]. Alshomrani et al. [21] discussed the 3D Darcy-Forchheimer model with carbon nanotubes and homogeneous-heterogeneous reactions. The flow of the viscous nanofluid with Darcy-Forchheimer effect past a curved surface is studied by Saif et al. [22]. Seth et al. [23] scrutinized numerically the flow of carbon nanotubes past a permeable Darcy-Forchheimer media in a rotating frame and many therein [24-28].

The impact of non-Newtonian fluids in the industry is more dominating in comparison to Newtonian fluids owing to their utility in varied applications [29]. Examples of non-Newtonian fluids may embrace coal water, paints, asphalt, toothpaste, shampoo, and jellies etc. [30].

Owing to the different nature of non-Newtonian fluids, numerous mathematical models are anticipated to meet their respective characteristics. The equations symbolizing these models are relatively more complex than Newtonian fluid models. Amongst these Powell Eyring fluid model is considered to be more effective because of its vast usage in chemical processes. This fluid model is erected by utilizing the kinetic theory of liquids in lieu of empirical relation. Nevertheless, at low/high shear stresses it behaves like Viscous fluid [31]. Moreover, Eyring Powell model is considered to be more accurate and trustworthy in assessing the fluid time scale at varied polymer concentrations [32]. Existing literature highlighting the various aspects of Eyring Powell fluid may include a study by Alshomrani et al. [33] who anticipated the flow of Eyring Powel nanofluid past a bi-directional stretching sheet and concluded that heat transfer rate triggered for improved values of activation energy. The flow of Eyring Powell nanofluid flow over a stretched surface are studied by Eldabe et al. [34] with the remark that velocity of the fluid is obstructed by high values of Eyring Powell parameter. Gholinia et al. [34] studied the flow of Eyring Powell nanofluid with slip condition and homogenous-heterogeneous reactions over a rotating disk. The flow of Eyring Powell nanofluid containing Ferrous oxide and aluminum oxide nanoparticles with Cattaneo-Christov heat flux is examined by Upadhya et al. [35]. Some more recent investigation highlighting Eyring Powell fluid flow may be found at [36-40].

From the aforementioned deliberations, it is comprehended that nanofluids are essentials in many engineering processes and to yield high-quality gadgets keeping in view economic efficacy. Furthermore, it is understood from the above deliberations that presented mathematical model is inimitable and no such exploration is undertaken in the literature before. Thus, the prime objective of the present study is to investigate the 3D Eyring Powell nanofluid flow past a nonlinear stretched surface under in a Darcy- Forchheimer porous media. Moreover, the novelty of the presented problem is improved by the addition of impacts of nonlinear thermal radiation, chemical reaction with zero mass flux condition. None of the above quoted and even existing literature simultaneously analyzed such effects. Analytical solution of the problem is acquired by engaging the Homotopy Analysis Method [41-44].

Chapter 2

Preliminaries

This section contains standard definitions, concepts and basic laws which are helpful in understanding the works in the second and third chapters.

2.1 Fluid

A material that can flow and continuously deforms under an impact of shear stress. Mercury, shampoos, cooking oil, blood and oxygen are some of its examples.

2.2 Fluid mechanics

The class of mecahnics deals with the characteristics of fluids. It can be classified into two subclasses.

2.2.1 Fluid statics

It investigates the attributes of liquids in stationary state.

2.2.2 Fluid dynamics

It investigates the attributes of liquids in the state of motion.

2.3 Flow

Flow is characterized as a material that deforms smoothly and fluently under the impacts of various kinds of forces. Flow is further divided into two major subclasses.

2.3.1 Laminar flow

Laminar flow is obtained when the fluid flows in regular paths, with no interruption between the layers.

2.3.2 Turbulent flow

Turbulent flow is obtained when the fluid particles have irregular velocity in the flow field.

2.4 Viscosity

It is the primary characteristic of fluid that measures the fluid's resistance to flow when numerous forces are acting on it. Mathematically, can be represented as follows:

$$\text{viscosity } (\mu) = \frac{\text{shearstress}}{\text{gradient of velocity}}. \tag{2.1}$$

2.4.1 Dynamic viscosity

It is define as the measure of fluid resistivity to flow. Its unit is kg/ms.

2.4.2 Kinematic viscosity

The ratio of the absolute viscosity of the fluid (μ) to the fluid density (ρ) is recognised as kinematic viscosity. Mathematically, it is represented by

$$\nu = \frac{\mu}{\rho}. \tag{2.2}$$

In SI system is $\frac{m^2}{s}$.

2.5 Newtonian fluids

Fluids that satisfy the Newton's law of viscosity and the value of μ is constant. In these fluids shear force (τ_{yx}) is proportional linearly to the gradient of velocity $\left(\frac{du}{dy}\right)$. Alcohol, water, glycerine and kerosene are common examples of this fluids.

2.6 non-Newtonian fluids

Fluids that doesnot satisfy the Newton's law of viscosity. Here, nonlinear and direct relationship exists between shear stress and gradient of velocity. Mathematically

$$\boldsymbol{\tau}_{yx} \propto \left(\frac{du}{dy}\right)^n, \; n \neq 1, \tag{2.3}$$

or

$$\boldsymbol{\tau}_{yx} = \eta \frac{du}{dy}, \; \eta = s\left(\frac{du}{dy}\right)^{n-1}, \tag{2.4}$$

where η is termed as apparent viscosity, $\boldsymbol{\tau}_{yx}$ the shear stress, s denotes consistency index, and n is the flow behaviour index. For $n = 1$, Eq. (2.4) represents the Newton's law of viscosity. Yougurt, honey and mayonnaise exhibits the non-Newtonian fluid behavior.

2.7 Newton's law of viscosity

Liquids which show the direct and linear corrspondence between velocity gradient and shear stress. Mathematically, it can be represented as follows:

$$\tau_{yx} \propto \frac{du}{dy}, \tag{2.5}$$

or

$$\tau_{yx} = \mu\left(\frac{du}{dy}\right), \tag{2.6}$$

in which τ_{yx} indicate the shear force applied on the fluid's element and μ indicate the proportionality constant.

2.8 Density

Mass of a material per unit volume, named as density. This quantity is used to calculate that how much stuff of a material present in a unit volume.

Mathematically, expessed as follows:

$$\rho = \frac{M}{V}, \tag{2.7}$$

where M is the mass of the substance and V is the volume. In SI system units it is calculated as kg/m^3.

2.9 Pressure

Pressure is defined as force employed on a surface per unit area.

Mathematically pressure is given by:

$$P = \frac{F_1}{A}. \tag{2.8}$$

The SI unit of pressure is Nm^{-2}.

2.10 Porous surface

It is a material which made out of pores, over which fluid or gas can travel through. Few examples are biological tissues, cork and rocks. Sponges, fabrics, ceramics and foams are also gathered for the purpose of porous media.

2.11 Porosity

The measure of spongy space in a porous substance is known as porosity.

2.12 Permeability

It is the strenght of a porous substance to allow fluid to travel through it. Those materials which have low porosity are minor permeable while materials having large pores are easily permeated and have high porosity.

2.13 Mechanism of heat flow

A form of energy that moves to colder area from hotter is said to be heat. Flow of heat takes place between two objects when they are of different temperatures. The transfer of heat occurs through any one of the following three ways:

2.13.1 Conduction

A phenomenon in which heat moves from warmer to cooler areas in liquids and solids because of the collisions of free electrons and molecules is called conduction. In this process molecules do not move for heat transfer to take place. Mathematically

$$\frac{\boldsymbol{q}}{A} = k\left(\frac{T_1 - T_2}{X_1 - X_2}\right) = k\frac{\Delta T}{\Delta X}, \tag{2.9}$$

where

$$\boldsymbol{q} = -kA\frac{dT}{dx}, \tag{2.10}$$

in which $\boldsymbol{q}$ represents the heat flow, A the area of the surface, k the thermal conductivity, T_1 temperature is greater than T_2, $\frac{dT}{dx}$ denotes the temperature gradient and minus sign indicates that heat is conducted from higher to lower temperature.

2.13.2 Radiation

Radiation is a process where heat flows to colder from hotter region as a result of the electromagetic waves. This phenomenon plays vital role in heat transfer in vaccum. Mathematically

$$\boldsymbol{q} = e\sigma^* A\left(\Delta T\right)^4, \tag{2.11}$$

where $\boldsymbol{q}$ denotes the heat transfer, e for emissivity of the system, σ^* for Stephen-Boltzmann's constant, A for area and $(\Delta T)^4$ for the temperature difference between two systems of fourth power.

2.13.3 Convection

Mechanism where by heat flows from hot to cold area of liquids or gases due to the movement of molecules is said to be convection. Mathematically,

$$q = hA\left(T_s - T_\infty\right), \tag{2.12}$$

where h is coefficient heat transfer (convective), T_s for system temperature, A for area and T_∞ for the ambient temperature.

2.14 Convective boundary conditions

Convective boundary conditions are some time called Robin boundary conditions.These kind of conditions are usually define on wall (surfaces). Mathematically

$$k\left(\frac{\partial T}{\partial m_i}\right)_{x_i} = h\left(T_f(x_i,t) - T_w(x_i,t)\right), \tag{2.13}$$

This equation says that condition is equal to convection. where h indicates the coefficient of heat transfer (convective) , x_i is the coordinate at the boundary, T_f the convective fluid temperature and T_w represents wall temperature.

2.15 Nanofluid

A liquid that has very small particles in it (called nanometer particles) is said to be Nanofluid. These liquids are formed by the colloidal suspensions of nanoparticles in the conventional liquid. The nanoparticles employed in nanofluids typically are nanotubes, oxides and metals. Most ordinary base fluids are oil and water.

2.16 Powell Eyring fluid

This fluid falls in class of non-newtonian fluids which have the properties of shear thinning fluids. Initially, it was extracted from kinetic theory of fluids instead of obtaining it from the empirical relation. Furthermore, it accordingly brings down to newtonian fluid for small and high shear rates. The Powell Eyring fluid model explains characteristics of shear thinning fluids. An appropriate example of Powell Eyring fluid would be human blood. The cauchy stress tensor is stated as follows:

$$T = -pI + T_{ij}, \tag{2.14}$$

in which, extra stress tensor T_{ij} is

$$T_{ij} = \mu \frac{\partial u_i}{\partial x_j} + \frac{1}{\beta} \sinh^{-1} \left(\frac{1}{d_1} \frac{\partial u_i}{\partial x_j} \right), \tag{2.15}$$

with d_1 and β are the Eyring Powell fluid characteristics, μ is dynamic visocsity, I is Identity Tensor and p is Pressure.

2.17 Darcy's law

It interprets the flow of a liquid through a spongy medium. This law was originated and dependent on the consequences of analysis on the flow of water across the beds of sand. It additionally models the scientific basis of fluid permeability needed in the Geo sciences.

2.18 Darcy Forchheimer Law

Movements in spongy medium with Reynolds numbers greater than 10, and in which inertial effects are prominant. So, this inertial term is add on the Darcy's equation and is called as Forchheimer term. This term represents the non-linear behavior of the pressure difference vs flow data.

$$\frac{\partial p}{\partial x} = \frac{\mu}{k^*} \upsilon_f - \frac{\rho}{k_1} \upsilon_f^2, \tag{2.16}$$

where k_1 represents inertial permeability and υ_f represents forchheimer velocity.

2.19 Non-dimensional numbers

2.19.1 Reynolds number (Re)

The significant dimensionless number which is used to recognize that either the flow is laminar or is turbulent. It describes inertial to viscous forces ratio. Mathematically, this number is expressed as:

$$\begin{aligned} \mathrm{Re} &= \frac{\text{inertial forces}}{\text{viscous forces}}, && (2.17) \\ &= \frac{v \times L}{\nu}. && (2.18) \end{aligned}$$

Here, v depicts the velocity of fluid, L describe the characteristic length and ν represent kinematic viscosity. Reynolds number are utilized to describe distinct flow behaviours (laminar or turbulent flow) within a similar fluid. Laminar flow arises at small Reynolds number, in which we can note that viscous effects are eminent. Turbulent flow arises at high Reynolds number, where inertial effects are eminent.

2.19.2 Prandtl number (Pr)

Momentum diffusivity to the thermal diffusivity ratio is termed as Prandtl number. Mathematically, it can be written as

$$\begin{aligned} \mathrm{Pr} &= \frac{\nu}{\alpha^*}, && (2.19) \\ &= \frac{\mu c_p}{k}, && (2.20) \end{aligned}$$

in which μ denotes the dynamic viscosity, c_p represent the specific heat and k stands for thermal conductivity.

2.19.3 Radiation parameter (Rd)

It is define as the relative contribution of conduction to the thermal radiation transfer, which can be expressed as follows:

$$Rd = \frac{4\sigma^* T_\infty^3}{kK}, \tag{2.21}$$

where K is the mean absorption coefficient, k stands for temperature dependent thermal conductivity, T_∞ for ambient temperature and σ^* denotes the Stefan-Boltzmann constant.

2.19.4 Skin friction coefficient (C_f)

Liquid passing over a surface experiences certain amount of drag that is known as Skin friction. It takes place between the flowing liquid and the solid's surface that causes reduction in the rate of flow of fluid. Mathematical expression for Skin friction is given as follows:

$$C_f = \frac{\tau_w}{\frac{1}{2}\rho U_w^2}, \tag{2.22}$$

in which τ_w demonstrate wall shear stress, ρ represents the density and U_w denotes the velocity.

2.19.5 Nusselt number (Nu_L)

This dimensionless number that represents the relationship among convection and conduction heat transfer coefficients at the boundary is known as Nusselt number. Mathematically

$$Nu_L = \frac{h\Delta T}{k\Delta T/L} = \frac{hL}{k}, \tag{2.23}$$

where h, L and k represent heat transfer coefficient (convective), characteristic length and thermal conductivity respectively.

2.19.6 Biot number (γ)

The ratio of internal diffusion resistivity to external convection resistance. Mathematically, it is represented as follows:

$$\gamma = \frac{hL}{k}, \tag{2.24}$$

where k and h represent the thermal conductivity and heat transfer coefficient (convective) respectively.

2.19.7 Thermophoresis parameter (Nt)

Thermodiffusion is utilized to prevent the mixing of different mobile particles of liquid due to a pressure gradient or separate the mixture of particles after mixing up due to the presence of thermal gradients.

Thermophoresis is positive for cold surface and it is negative for a hot surface.

Mathematically

$$Nt = \frac{(\rho c)_p D_T (T_f - T_\infty)}{(\rho c)_f \ v T_\infty}, \tag{2.25}$$

where T_f and T_∞ denotes the convective fluid temperature and ambient temperature, D_T stand for thermophoretic coefficient and v represents the kinematic viscosity.

2.19.8 Brownian motion parameter (Nb)

A random movement of nanoparticles in base liquid which occurs due to size of the nanoparticles is called as brownian motion. It is a nanoscale phenomenon that exhibits the thermal influences of nanofluid.

Mathematically

$$Nb = \frac{(\rho c)_p D_B \cdot (C_\infty)}{(\rho c)_f v}, \tag{2.26}$$

in the above equation τ is the ratio of effective heat and heat capacity of the nanoparticles and fluid respectively, v denotes the kinematic viscosity. C_w stands for wall's concentration, C_∞ stands for ambient concentration and and D_B represents brownian diffusion coefficient.

2.19.9 Schmidt number (Sc)

This dimensionless quantity can be expressed with the ratio of non-newtonian viscosity (kinematic) to mass diffusivity.

Mathematically

$$Sc = \frac{\nu}{D_B}, \tag{2.27}$$

where ν represents the kinematic viscosity and D_B stand for mass diffusivity.

2.19.10 Forchheimer number (Fr)

The Forchheimer number is proposed to identify different flow patterns. This number is determined with the ratio of pressure gradient to the viscous resistance.

Mathematically

$$Fr = \frac{k^* \rho v \beta^*}{\mu}, \tag{2.28}$$

with β^*non-Darcian coefficient and $k^*$the permeability of porous medium.

2.19.11 Chemical reaction parameter (δ_1)

The non-dimensional number used to measure the strenght of chemical reaction rate is called chemical reaction parameter and can be written as:

$$\delta_1 = \frac{k_c}{a} (x + y)^{1-n}, \tag{2.29}$$

whence k_c and n represents the rate constant and power law index.

2.20 Conservation laws

A measurable quantity that remains unchanged with the progression of time in an isolated system is called conserved quantity and the law which deals with this quantity is recognized as conservation law. The conservation laws that are used for the flow specification in the subsequential analysis are given below.

2.20.1 Mass conservation law

Conservation law for mass defines that the whole mass in any closed system will remain conserved. Mathematically

$$\frac{D\rho}{Dt} + \rho\boldsymbol{\nabla}.\mathbf{V} = 0, \tag{2.30}$$

or

$$\frac{\partial\rho}{\partial t} + (\mathbf{V}.\boldsymbol{\nabla})\,\rho + \rho\boldsymbol{\nabla}.\mathbf{V} = 0, \tag{2.31}$$

or

$$\frac{\partial\rho}{\partial t} + \boldsymbol{\nabla}.\,(\rho\mathbf{V}) = 0. \tag{2.32}$$

The above equation is known as equation of continuity. For the steady flow Eq. (2.32) becomes

$$\boldsymbol{\nabla}.\,(\rho\mathbf{V}) = 0, \tag{2.33}$$

and for the incompressible fluid, Eq. (2.33) will be stated as:

$$\boldsymbol{\nabla}.\mathbf{V} = 0. \tag{2.34}$$

2.20.2 Momentum conservation law

It is defined as the total linear momentum of a closed system is constant. Generally, it is given by

$$\rho\frac{D\mathbf{V}}{Dt} = \operatorname{div}\boldsymbol{\tau} + \rho\mathbf{b}, \tag{2.35}$$

where $\boldsymbol{\tau} = -\mathbf{pI} + \mathbf{S}$, the Cauchy stress tensor, $\frac{D}{Dt}$ represents the material time derivative and $\mathbf{b}$ stands for body force.

2.20.3 Law of energy conservation

This law is also known as energy equation and is described as total energy is conserved at the whole system. For nanofluids it is specified by

$$\rho_f c_f \frac{DT}{Dt} = \tau^*.L^* + k\nabla^2 T + \rho_p c_p \left(D_B \nabla C.\nabla T + \frac{DT}{T_\infty} \nabla T.\nabla T \right), \tag{2.36}$$

in which ρ_f represents the base fluid density, c_f stands for specific heat of base fluid, τ^* the stress tensor, L^* for the strain tensor, ρ_p denotes the density of nanoparticles, D_B denotes the Brownian diffusivity, D_T represents the thermophoretic diffusion coeffiecient, k denotes the thermal conductivity and T for temperature.

2.20.4 Law of conservation of concentration

For nanoparticles, the volume fraction equation is

$$\frac{\partial C}{\partial t} + \mathbf{V}.\boldsymbol{\nabla}\mathbf{C} = -\frac{1}{\rho_p}\boldsymbol{\nabla}.\mathbf{j}_p, \tag{2.37}$$

$$\mathbf{j}_p = -\rho_p D_B \nabla C - \rho_p D_T \frac{\nabla T}{T_\infty} \tag{2.38}$$

$$\frac{\partial C}{\partial t} + \mathbf{V}.\boldsymbol{\nabla}\mathbf{C} = \mathbf{D}_B\boldsymbol{\nabla}^2\mathbf{C} + \mathbf{D}_T\frac{\boldsymbol{\nabla}^2 T}{T_\infty}. \tag{2.39}$$

Here, D_B, C, T and D_T stand for Brownian diffusivity, nanoparticle concentration, temperature and thermophoretic coefficients respectively.

2.21 Thermal diffusivity

It is a material specific property for describing the unsteady conductive heat flow. This value describes how speedily a material respond to change in temperature. It is the ratio of thermal conductivity to specific heat capacity and density. Mathematically,

$$\alpha^* = \frac{k}{\rho c_p}, \tag{2.40}$$

where k the thermal conductivity, c_p the specific heat capacity and ρ the density.

2.22 Thermal conductivity

It is the measurement of the capacity of a substance to conduct heat . The fourier law of heat conduction " The amount of heat transfer rate (q) through a material of unit thickness (d) times unit cross section area (A) and unit temperature difference (ΔT)". Mathematically, written as:

$$k = \frac{qd}{A(\Delta T)}. \tag{2.41}$$

In SI system thermal conductivity has unit $\frac{W}{m.K}$.

2.23 Homotopic solutions

Homotopy is one of the basic concept of topology. It is stated as continous mapping in which one function can be constantly transformed into the another function. If one function h_1 and the other h_2 are maps from the topological space D with the other topological space E, then there exists a continous mapping H such that

$$H : D \times [0\ , 1] \rightarrow E, \tag{2.42}$$

where $d \in D$ and

$$F(d, 0) = h_1(x), \tag{2.43}$$

$$F(d, 1) = h_2(x). \tag{2.44}$$

That mapping H is termed as homotopy.

2.24 Homotopy analysis method

The Homotopy Analysis method (HAM) is involved to find the series solutions of highly non-linear problems. This method presents us with convergent series solutions for highly nonlinear systems. To have the basic concept of homotopy analysis method, lets suppose a differential

equation

$$\otimes [e(x)] = 0, \tag{2.45}$$

here $\otimes$ represents nonlinear operator, $e(x)$ is not known function while x is for the independent variable. Zeroth-order problem would be written as follows:

$$(1 - Þ) \mathrm{L} [\breve{e}(x; Þ) - e_0(x)] = Þ\hbar \otimes [\breve{e}(x; Þ)], \tag{2.46}$$

in this $e_0(x)$ is for the initial approximation, L represents the auxiliary linear operator, $Þ \in [0, 1]$ symbolizes an embedding parameter, $\hbar$ stands for nonzero auxiliary parameter and $\breve{e}(x; Þ)$ denotes the not known function of x and Þ.

Taking $Þ = 0$ and $Þ = 1$ one has

$$\breve{e}(x; 0) = e_0(x) \quad \text{and} \quad \breve{e}(x; 1) = e_0(x). \tag{2.47}$$

The solution $\breve{e}(x; Þ)$ differ from initial approximation $e_0(x)$ to the expected final solution $e(x)$ when Þ vary from 0 to 1. Utilizing taylor series expansion, we have

$$\breve{e}(x; Þ) = e_0(x) + \sum_{m=1}^{\infty} e_m(x) Þ^m, \quad e_m(x) = \frac{1}{m!} \frac{\partial^m \breve{e}(x; Þ)}{\partial Þ^m}\bigg|_{Þ=0}. \tag{2.48}$$

For $Þ = 1$, we get

$$e(x) = e_0(x) + \sum_{m=1}^{\infty} e_m(x). \tag{2.49}$$

Differentiate m times the zeroth deformation with respect to Þ, and divide it by $m!$ and lastly putting $Þ = 0$, we obtain the mth order equation

$$\mathrm{L} [e_m(x) - \chi_m e_{m-1}(x)] = \hbar \mathcal{R}_m(x), \tag{2.50}$$

$$\mathcal{R}_m(x) = \frac{1}{(m-1)!} \frac{\partial^m \otimes [\breve{e}(x; Þ)]}{\partial Þ^m}\bigg|_{Þ=0}, \tag{2.51}$$

where

$$\chi_m = \begin{cases} 0, & m \leq 1 \\ 1, & m > 1 \end{cases}. \tag{2.52}$$

Chapter 3

Darcy-Forchheimer 3D flow of Williamson nanofluid over a convectively heated nonlinear stretching surface

3.1 Mathematical formulation

In this chapter, we consider a steady, 3D Williamson nanofluid flow bounded by nonlinear stretchable surface in existence of convective heat and zero mass flux conditions. The fluid flow comply with Darcy-Forchhiemer spongy medium. Here, u, v and w are velocities along (x, y, z) directions respetively. The stretching is in the $x-$ and $y-$ directions with respective velocities $U_w(x, y) = a(x + y)^n$ and $V_w(x, y) = b(x + y)^n$ whereas $z-$ in the normal direction, with $a, b, n > 0$. T and C are the temperature of fluid and nanofluid's concentration. Likewise, C_∞ and T_∞ represents the ambient concentration and temperature. The governing system representing the given scenario is given as:

$$u_x + v_y + w_z = 0, \tag{3.1}$$

$$uu_x + vu_y + wu_z = \nu u_{zz} + \sqrt{2}\nu\Gamma\left(u_z u_{zz}\right) - \frac{\nu}{k^*}u - Fu^2, \tag{3.2}$$

$$uv_x + vv_y + wv_z = \nu v_{zz} + \sqrt{2}\nu\Gamma\left(v_z v_{zz}\right) - \frac{\nu}{k^*}v - Fv^2, \tag{3.3}$$

$$uT_x + vT_y + wT_z = \alpha^*\left(T_{zz}\right) + \frac{(\rho c)_p}{(\rho c)_f}\cdot\left(D_B\left(T_z C_z\right) + \frac{D_T}{T_\infty}\left(T_z\right)^2\right), \tag{3.4}$$

$$uC_x + vC_y + wC_z = D_B\left(C_{zz}\right) + \frac{D_T}{T_\infty}\left(T_{zz}\right), \tag{3.5}$$

with the boundary conditions

$$\begin{gathered} u = U_w,\ v = V_w, w = 0, -kT_z = h_f\left(T_f - T\right), \\ D_B C_z + \frac{D_T}{T_\infty}T_z = 0 \text{ at } \ \mathrm{z} = 0, \\ u \to 0,\ T \to T_\infty\ , C \to C_\infty \text{ as } z \to \infty. \end{gathered} \tag{3.6}$$

Dimensionless form of above mathematical model is obtained by utilizing following transformations:

$$\zeta = \sqrt{\left(\frac{a\left(n+1\right)}{2\nu}\right)}\left(x+y\right)^{\frac{(n-1)}{2}} z,\ \phi\left(\zeta\right) = \frac{C - C_\infty}{C_\infty},$$

$$\begin{aligned} u &= a\left(x+y\right)^n f'\left(\zeta\right),\ v = a\left(x+y\right)^n g'\left(\zeta\right),\ \ \theta\left(\zeta\right) = \frac{T - T_\infty}{T_f - T_\infty}, \\ w &= -\sqrt{\left(\frac{a\nu\left(n+1\right)}{2}\right)}\left(x+y\right)^{\frac{n-1}{2}}\left(\left(f+g\right) + \left(\frac{n-1}{n+1}\right)\zeta\left(f'+g'\right)\right). \end{aligned} \tag{3.7}$$

Here, satisfaction of Eq. (3.1) is inevitable. However, Eqs.$(3.2 - 3.6)$ reduce

$$f''' + \left(f+g\right)f'' - \left(\frac{2\cdot n}{n+1}\right)\left(f'+g'\right)f' + Wef''f''' - \left(\frac{2}{n+1}\right)\left(\lambda f' + Fr\left(f'\right)^2\right) = 0, \tag{3.8}$$

$$g''' + \left(f+g\right)g'' - \left(\frac{2\cdot n}{n+1}\right)\left(f'+g'\right)g' + Weg''g''' - \left(\frac{2}{n+1}\right)\left(\lambda g' + Fr\left(g'\right)^2\right) = 0, \tag{3.9}$$

$$\theta'' + \Pr\left((f+g)\,\theta' + Nb\theta'\phi' + Nt\theta'^{2}\right) = 0, \tag{3.10}$$

$$\phi'' + Sc\,(f+g)\,\phi' + \frac{Nt}{Nb}\theta'' = 0, \tag{3.11}$$

$$f(0) = 0, g(0) = 0, f'(0) = 1, g'(0) = \alpha,\ \acute{\theta}(0) = -\gamma\,(1-\theta(0)), Nb\phi'(0) + Nt\theta'(0) = 0, \tag{3.12}$$

$$f'(\infty) \to 0,\ g'(\infty) \to 0,\ \theta(\infty) \to 0,\ \phi(\infty) \to 0, \tag{3.13}$$

with

$$We = a\Gamma\sqrt{\frac{a\,(n+1)}{\nu}}\,(x+y)^{(3n-1)/2}, \lambda = \frac{\nu}{k^{*}a}\,(x+y)^{1-n},\ Nt = \frac{(\rho c)_p\, D_T\,(T_f - T_\infty)}{(\rho c)_f\,\nu T_\infty},$$

$$\Pr = \frac{\nu}{\alpha^{*}},\ Sc = \frac{\nu}{D_B}, Fr = \frac{C_b}{k^{*1/2}},\ Nb = \frac{(\rho c)_p\, D_B C_\infty}{(\rho c)_f\,\nu},\ \alpha = \frac{b}{a},\ \gamma = \frac{h}{k}\sqrt{\frac{\nu}{a}}. \tag{3.14}$$

Skin friction and local Nusselt number in dimensionless quantities are appended as follows:

$$C_{fx}\,\mathrm{Re}_x^{1/2} = \sqrt{\left(\frac{n+1}{2}\right)}\left(f''(0) + \frac{We}{2}f''^{2}(0)\right), \tag{3.15}$$

$$C_{fy}\,\mathrm{Re}_y^{1/2} = \alpha^{-3/2}\cdot\sqrt{\left(\frac{n+1}{2}\right)}\left(g''(0) + \frac{We}{2}g''^{2}(0)\right), \tag{3.16}$$

$$Nu_x\,\mathrm{Re}_x^{-1/2} = -\left(\frac{n+1}{2}\right)^{\frac{1}{2}}\theta'(0). \tag{3.17}$$

In the existence of zero mass flux condition, the Sherwood number is analogously vanish and Local Reynolds numbers are given as, $\mathrm{Re}_x = \frac{U_w}{\nu}(x+y)$ and $\mathrm{Re}_y = \frac{V_w}{\nu}(x+y)$.

3.2 Homotopic solutions

An analytical methodology called (HAM) Homotopy analysis method is involved to find out the convergent series solutions. This technique has an edge over the analytical methods because of following characteristics:

i) Independency from selection of large and small parameters.

ii) Convergence of series solution is guaranteed.

iii) Ample liberty for selection of linear operators and base functions.

Following this method, the initial approximations $(f_0, g_0, \theta_0, \phi_0)$ and relevant linear operators $(\mathrm{L}_f\ , \mathrm{L}_g\ , \mathrm{L}_\theta,\ \mathrm{L}_\phi)$ are expressed as follows:

$$f_0(\zeta) = (1 - \exp(-\zeta)), \qquad g_0(\zeta) = \alpha \cdot (1 - \exp(-\zeta)),$$
$$\theta_0(\zeta) = \left(\frac{\gamma}{1+\gamma}\right) \cdot \exp(-\zeta), \qquad \phi_0(\zeta) = -\frac{\gamma}{1+\gamma}\left(\frac{N_t}{N_b}\right) \cdot \exp(-\zeta), \tag{3.18}$$
$$\mathrm{L}_f\ = f_{\zeta\zeta\zeta} - f_\zeta,\ \mathrm{L}_g\ = g_{\zeta\zeta\zeta} - g_\zeta,\ \mathrm{L}_\theta\ = \theta_{\zeta\zeta} - \theta,\ \mathrm{L}_\phi\ = \phi_{\zeta\zeta} - \phi, \tag{3.19}$$

along with the properties

$$\begin{aligned}
\mathrm{L}_f\ (q_1 + q_2 \exp(\zeta) + q_3 \exp(-\zeta)) &= 0,\\
\mathrm{L}_g\ (q_4 + q_5 \exp(\zeta) + q_6 \exp(-\zeta)) &= 0,\\
\mathrm{L}_\theta\ (q_7 \exp(\zeta) + q_8 \exp(-\zeta)) &= 0,\\
\mathrm{L}_\phi\ (q_9 \exp(\zeta) + q_{10} \exp(-\zeta)) &= 0,
\end{aligned} \tag{3.20}$$

here q_j and $(j = 1 - 10)$ are described as optional constants.

3.3 Convergence analysis

The HAM is utilized to find the series solutions and is highly depended on supplementary parameters $\hbar_f, \hbar_g,\ \hbar_\theta$ and $\hbar_\phi$. These parameters are essential to regulate and manage the convergence area. The acceptable ranges of the supplementary parameters are $-1.50 \leq \hbar_f \leq -0.5$, $-1.50 \leq \hbar_g \leq -0.5$, $-1.50 \leq \hbar_\theta \leq -0.5$ and $-1.50 \leq \hbar_\phi \leq -0.5$. Table 3.1 is also erected to see the convergence of series solutions and it is identified that 25^{th} order of approximation is sufficient to form the series solutions. We can see that values obtained in the table are appropriately in sequence to the curves shown in Fig. 3.1. This also validates both numerical and graphical representation.

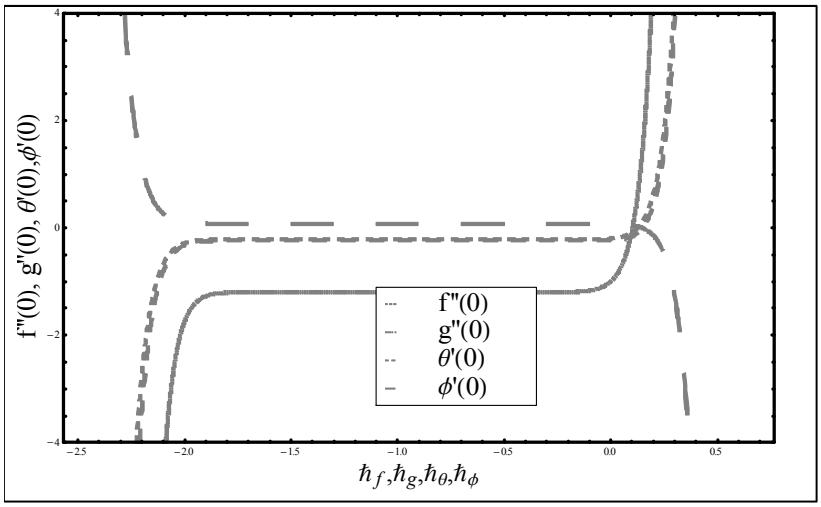

Fig 3.1 $\hbar-$ curves for f, g, θ and ϕ.

Table 3.1**:** Convergence of Homotopy series solutions for varied order of estimations.

Order of Approximation	$-f''(0)$	$-g''(0)$	$-\theta'(0)$	$\phi'(0)$
1	1.11671	0.20159	0.23166	0.07721
5	1.24100	0.20403	0.23076	0.07691
10	1.26950	0.20412	0.23002	0.07667
15	1.27120	0.20410	0.22983	0.07660
20	1.27140	0.20409	0.22977	0.07650
25	1.27150	0.20409	0.22975	0.07658
30	1.27150	0.20409	0.22975	0.07658

3.4 Results and discussions

This section addresses the impacts of distinct parameters on all involved distributions via numerous graphical illustrations. Figure 3.2 is sketched to portray the impact of λ, the porosity parameter on velocity field $f'(\zeta)$. Graph depicts that velocity distribution is an decreasing function of λ. This is because, the permeable medium influences the boundary layer, which prompts increasing velocity of the fluid. Because of this reality, the velocity diminishes with the escalation of a porosity parameter λ. Figure 3.3 illustrates that how Williamson parameter We

affects the velocity distribution $f'(\zeta)$. It is noted that for larger values of williamson parameter, the velocity distribution and its associated thermal thickness reduce. This number (We) is expressed as the ratio between relaxation to retardation time. By increasing this parameter, the relaxation time enhances. With this, the liquid viscosity increases and this results in decrease in velocity profile. Impact of Forchheimer number Fr on velocity distribution $f'(\zeta)$ is portrayed in figure 3.4. It is examined that for escalating values of Fr, decreasing behaviour of the velocity distribution is seen from figure 3.5. This is because, for the higher values of Fr lead to a resistance in a fluid flow. It is witnessed that the velocity profile $g'(\zeta)$ is diminishing function for higher values of Williamson parameter We. By increasing We parameter, the rise in relaxation time is observed and thus, the liquid viscosity increases and this results in decrease in velocity profile. In figure 3.6 influence of porosity parameter λ on the velocity field $g'(\zeta)$ is presented. It is examined that augmented values of λ lower velocity field. Physically existence of spongy media is to boost the resistance to liquid motion which provides decay in fluid velocity. Forchheimer number Fr effect is discussed in figure 3.7,which tells that for higher Forchheimer number Fr the velocity field $g'(\zeta)$ is reduced. Reason for this is that, higher values of Fr lead to a resistance in a liquid flow. Figure 3.8 is sketch to describe the effect of Williamson parameter We on the temperature distribution $\theta(\zeta)$. Escalating values of We causes increase in temperature distribution because of increase in resistance to the liquid flow. Figure 3.9 is portrayed to depict the effect of porosity parameter λ on the temperature distribution $\theta(\zeta)$. It is observed that temperature profile is escalates for larger values of λ. Naturally the resistance is observed in fluid movement because of the presence of permeable media which produces a decay in the fluid velocity. Hence an enhancemnt is observed in the temperature field. In figure 3.10 effect of Forchheimer number Fr is discussed on temperature field $\theta(\zeta)$. It is analyzed that for higher values of Fr shows increasing behaviour of temperature profile. Figure 3.11 shows that for greater values of Biot number γ, an enhancement in the temperature $\theta(\zeta)$ is witnessed. This is due to fact that, when the Biot number increases, higher convection takesplace which results in an increment in the temperature profile $\theta(\zeta)$. Figure 3.12 indicates the impact of thermophoresis parameter Nt on temperature $\theta(\zeta)$. It is observed that for larger values of Nt, increase in the temperature field and its related thermal layer thickness is seen. Smaller particles are pushed apart from hot area to cold area in the process of thermophoresis.

Consequently it boost the fluid temperature. In figure 3.13 effect of Williamson parameter We on concentration field $\phi(\zeta)$ is presented. Williamson parameter increases the fluid viscosity, as a result, when We values are raised, concentration distribution of fluid gets enhnaced. Figure 3.14 is portrayed to depict the effect of porosity parameter λ on concentration distribution $\phi(\zeta)$. An increase in concentration field is observed against gradual escalation in λ. Figure 3.15 demonstrates the impact of Forchheimer number Fr on concentration field. An increase in Fr causes upsurge in the concentration profile. Figure 3.16 is drawn to show impact of the Schmidt number Sc on concentration field. It is deduced that concentration profile is being reduced for larger values of Sc. Schmidt number is the ratio of momentum to mass diffusivities. With the increase of schmidt number Sc the mass diffusivities decreases and results in the depletion of concentration $\phi(\zeta)$. Figure 3.17 shows that how the Brownian motion N_B effect the concentration profile $\phi(\zeta)$. For higher value of Nb, the concentration profile is reduced. It is perceived that with increase in Nb random motion of macroscopic fluid particles and collision among themselves increase which ultimately reduces the concentration of the fluid. Figure 3.18 is portrayed to depict the effect of thermophoresis parameter Nt on concentration distribution $\phi(\zeta)$. An increase in concentration field is viewed against gradual escalation in Nt. In the phenomenon of thermophoresis, the tiny particles are pushed far from warm area towards the cold area. The reason behind this is that increasing the estimation of thermophoresis parameter, augmentation in the concentration profile $\phi(\zeta)$ is observed. Figure 3.19 is drawn to show the impact of Forchheimer number Fr and Williamson parameter We on Skin friction coefficient $\left(C_f \operatorname{Re}_x^{\frac{1}{2}}\right)$. It is observed that for greater values of Fr Skin friction decreases. Figure 3.20 express the effect of We and Fr on $\left(C_f \operatorname{Re}_y^{\frac{1}{2}}\right)$. It is concluded that for large values of Fr Skin friction diminishes. Figure 3.21 illustrate the effect of thermophoresis parameter Nt and Brownian motion Nb on Nusselt number. It is analyzed that nusselt number decreases for escalating values of Nt.

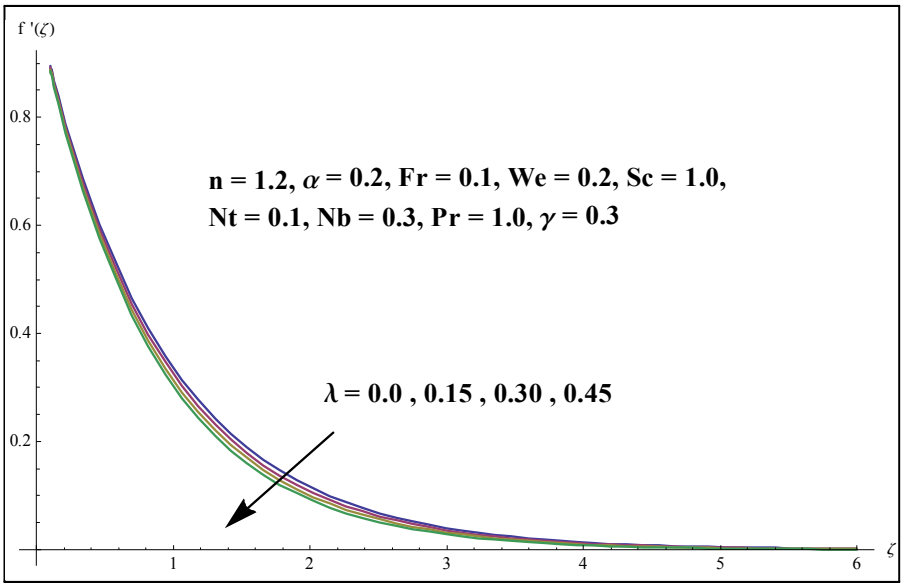

Fig. 3.2 Influence of λ on $f'(\zeta)$.

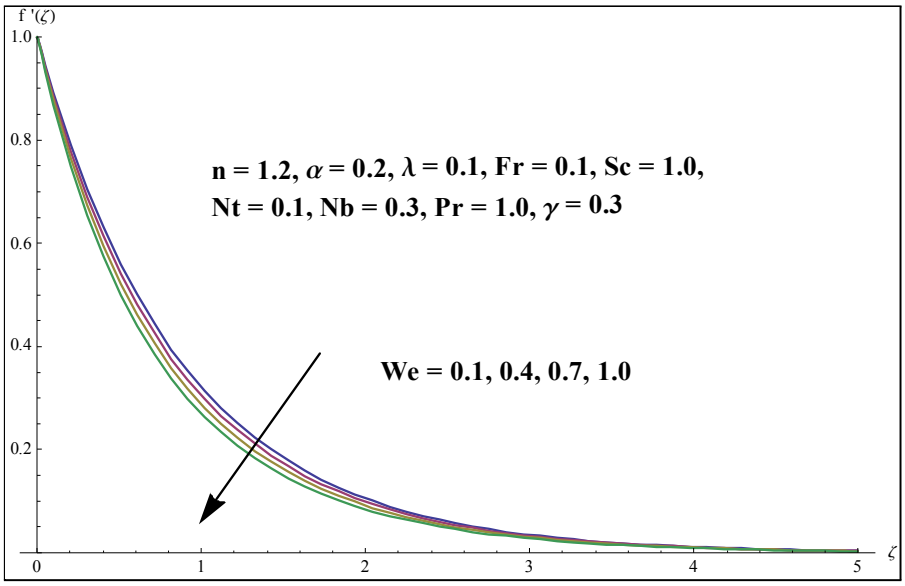

Fig. 3.3 Influence of We on $f'(\zeta)$.

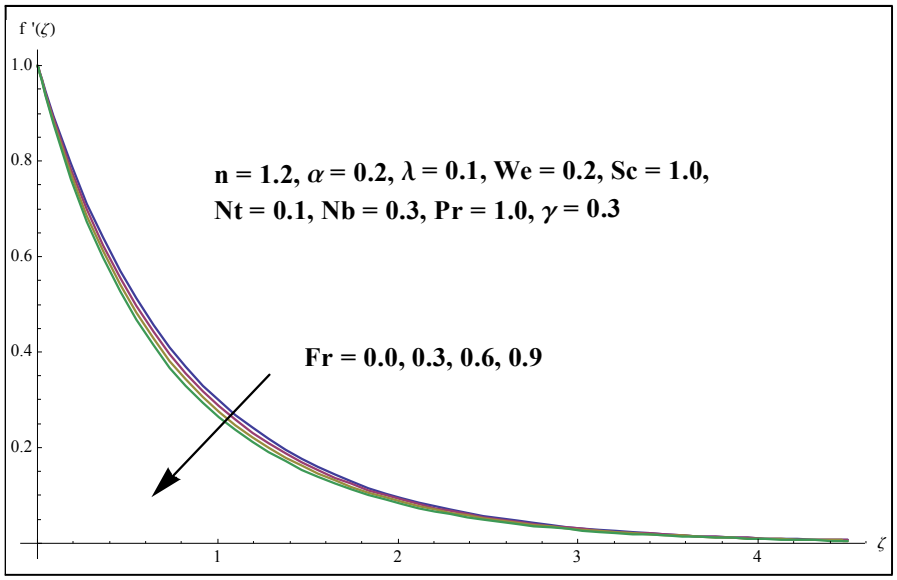

Fig. 3.4 Influence of Fr on $f'(\zeta)$.

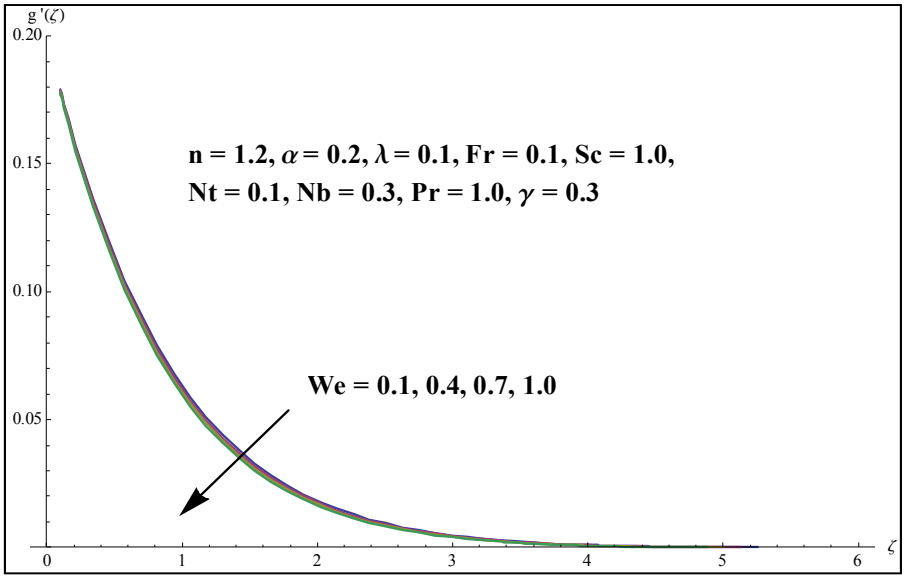

Fig. 3.5 Influence of We on $g'(\zeta)$.

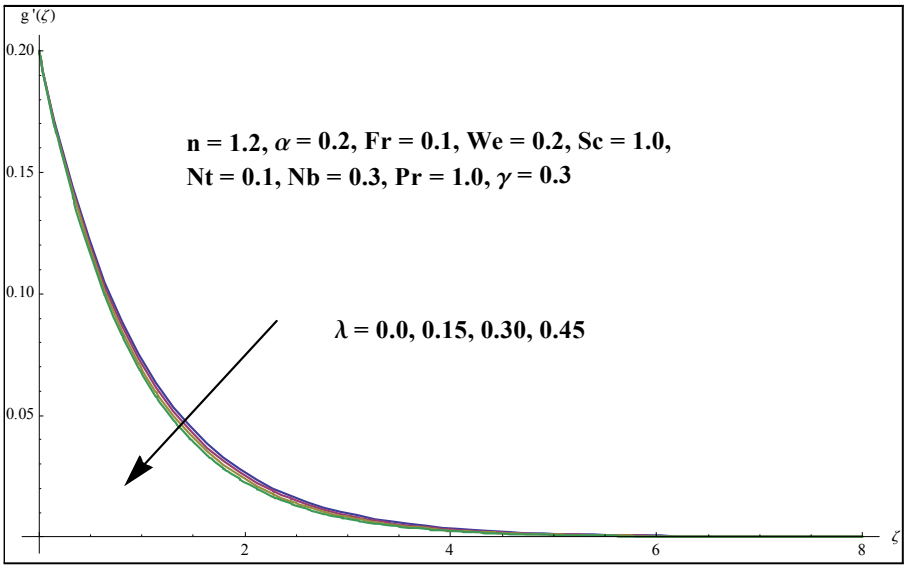

Fig. 3.6 Influence of λ on $g'(\zeta)$.

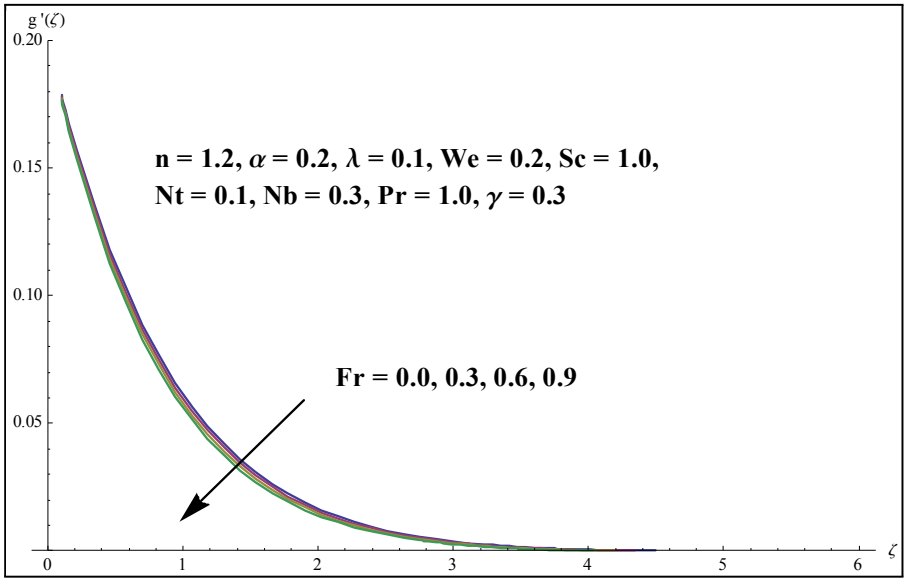

Fig. 3.7 Influence of Fr on $g'(\zeta)$.

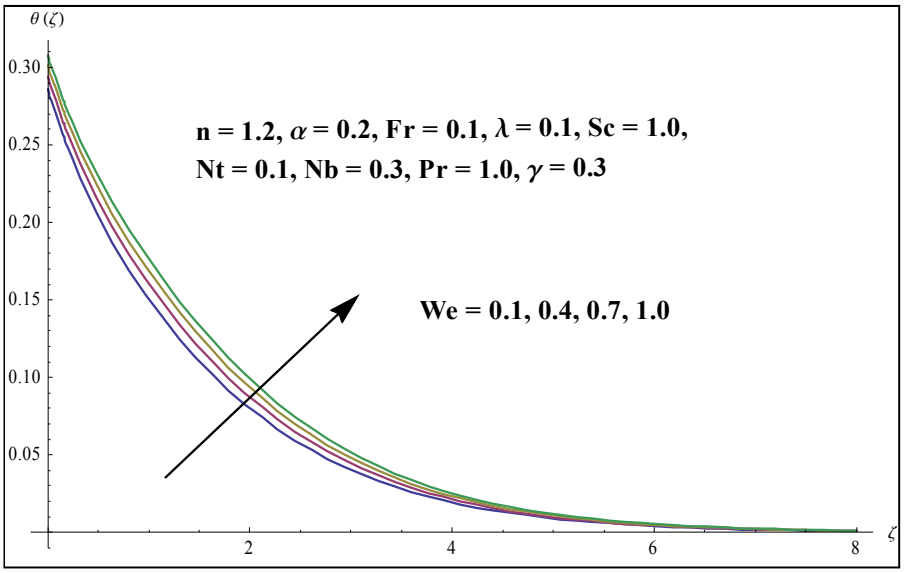

Fig. 3.8 Influence of We on $\theta(\zeta)$.

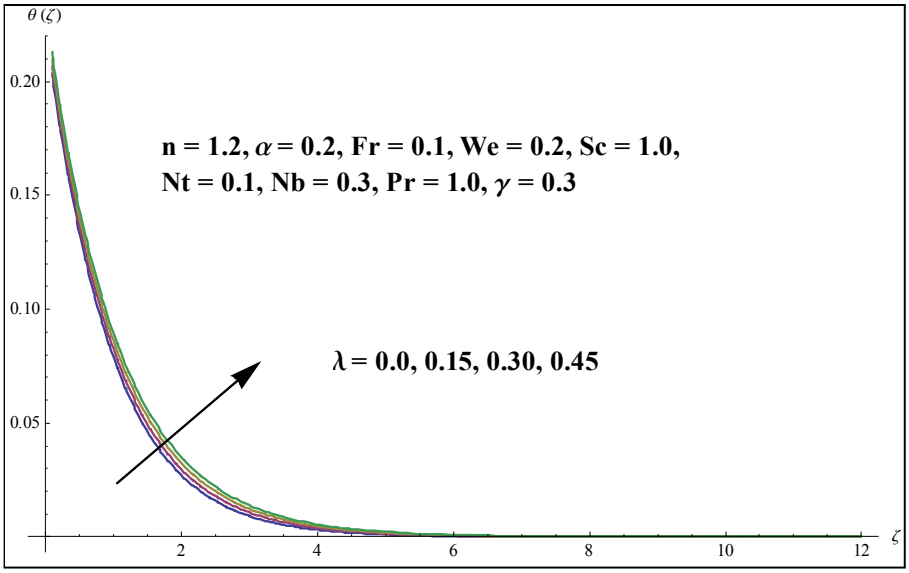

Fig. 3.9 Influence of λ on $\theta(\zeta)$.

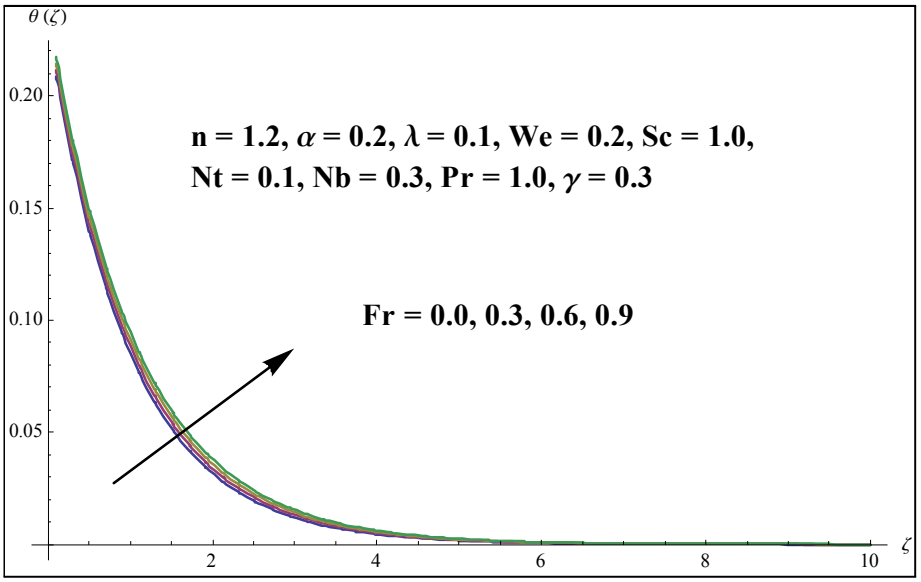

Fig. 3.10 Influence of Fr on $\theta(\zeta)$.

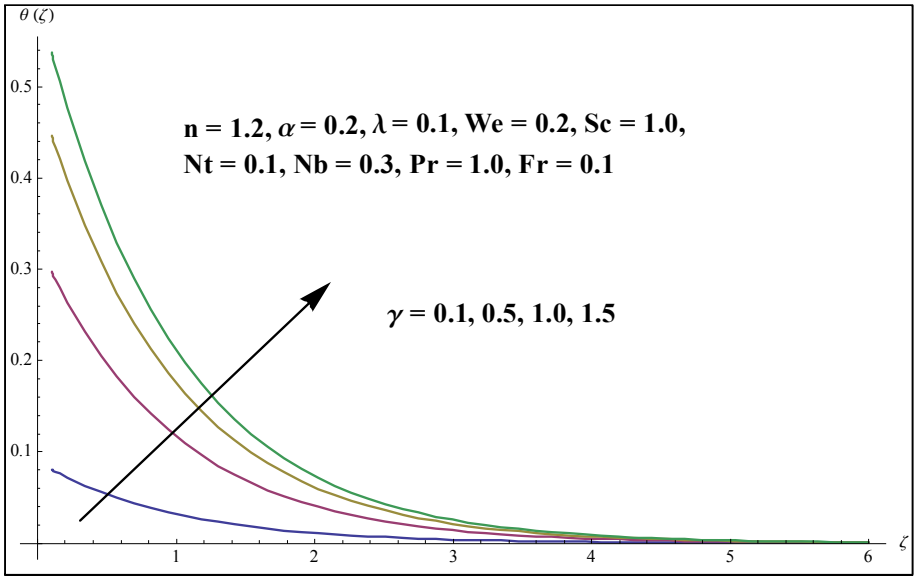

Fig. 3.11 Influence of γ on $\theta(\zeta)$.

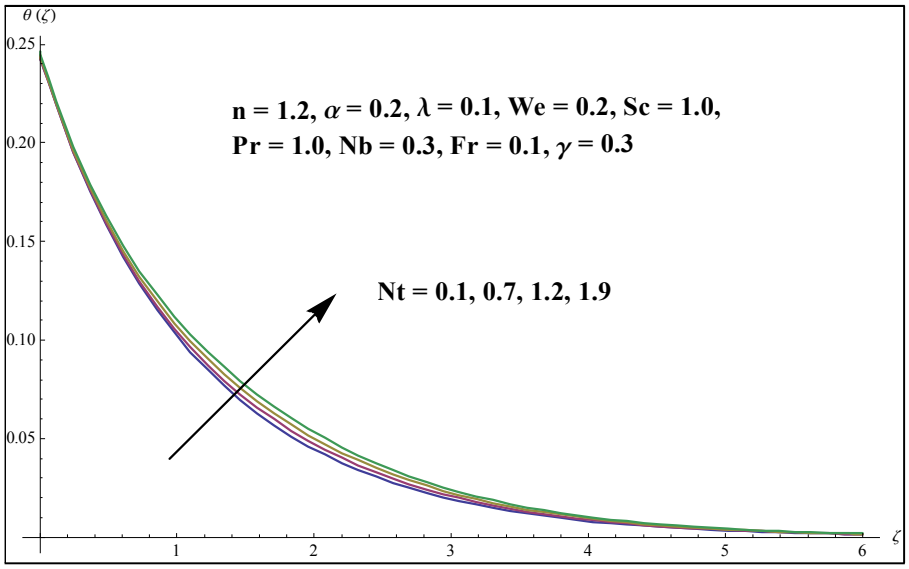

Fig. 3.12 Influence of Nt on $\theta(\zeta)$.

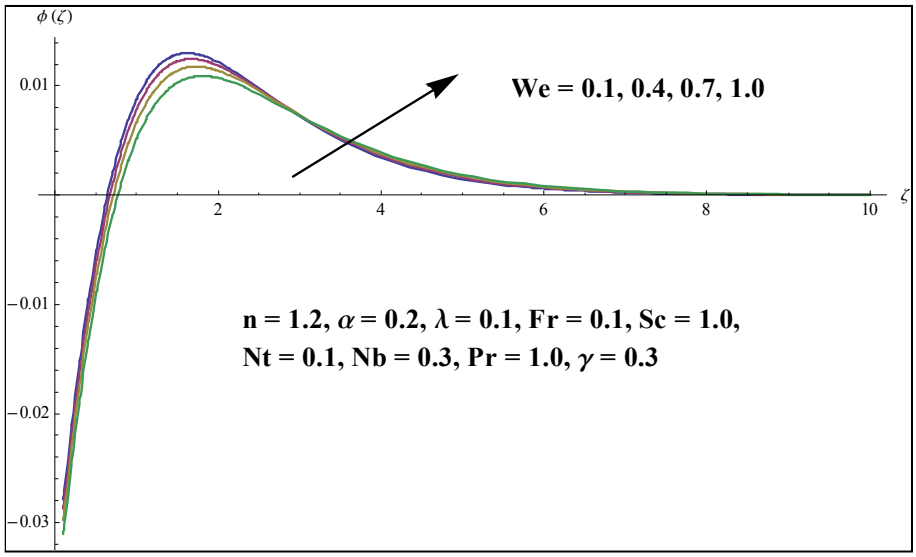

Fig. 3.13 Influence of We on $\phi(\zeta)$.

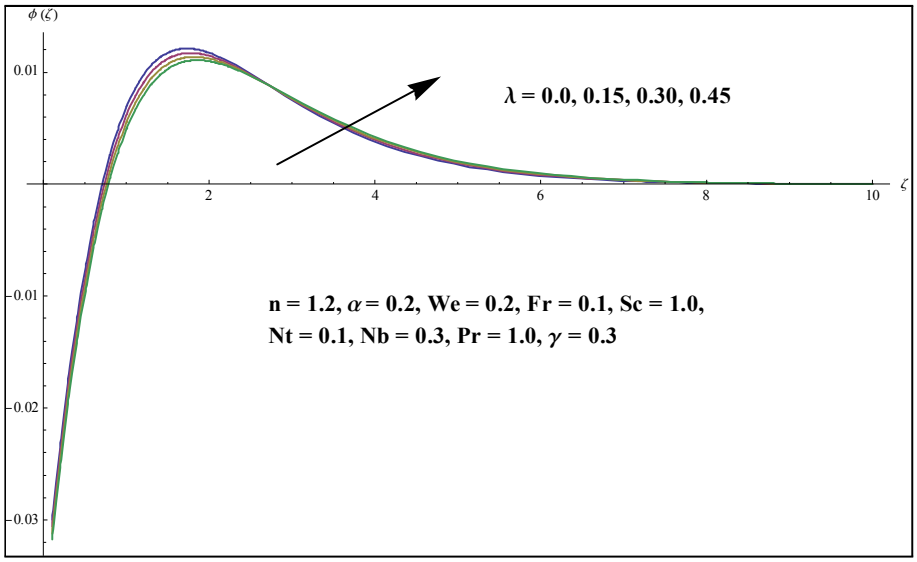

Fig. 3.14 Influence of λ on $\phi(\zeta)$.

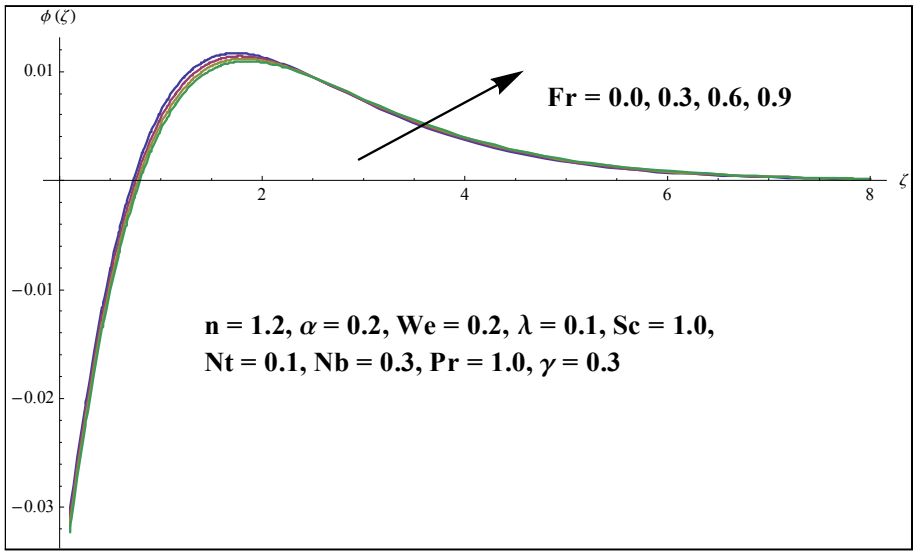

Fig. 3.15 Influence of Fr on $\phi(\zeta)$.

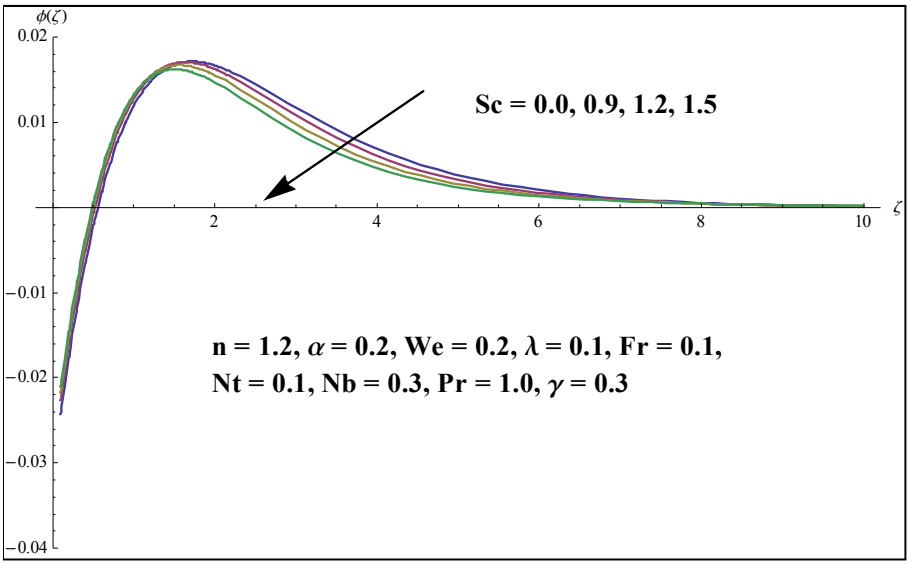

Fig. 3.16 Influence of Sc on $\phi(\zeta)$.

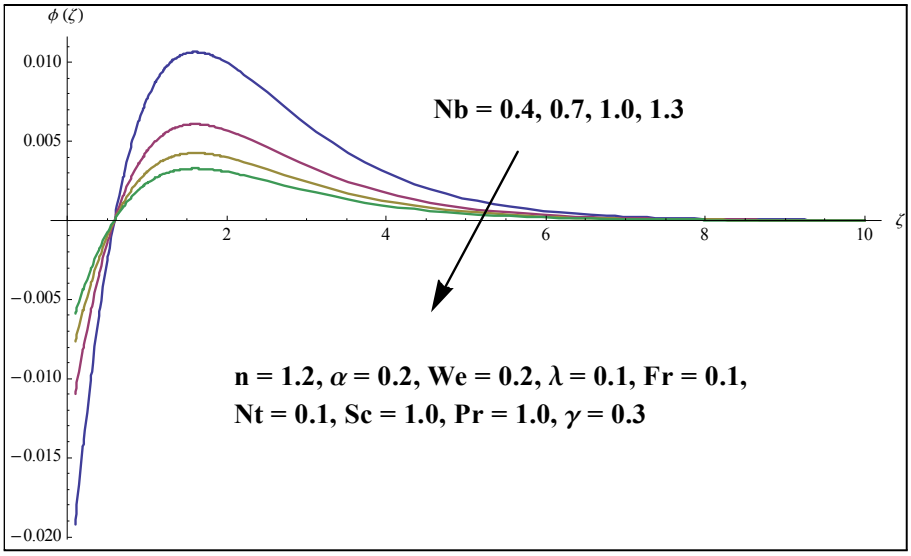

Fig. 3.17 Influence of Nb on $\phi(\zeta)$.

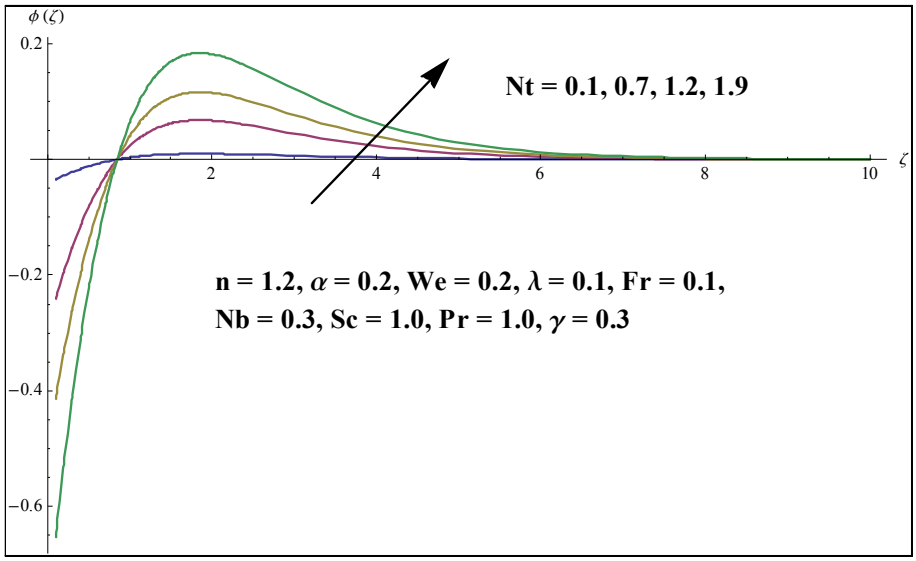

Fig. 3.18 Influence of Nt on $\phi(\zeta)$.

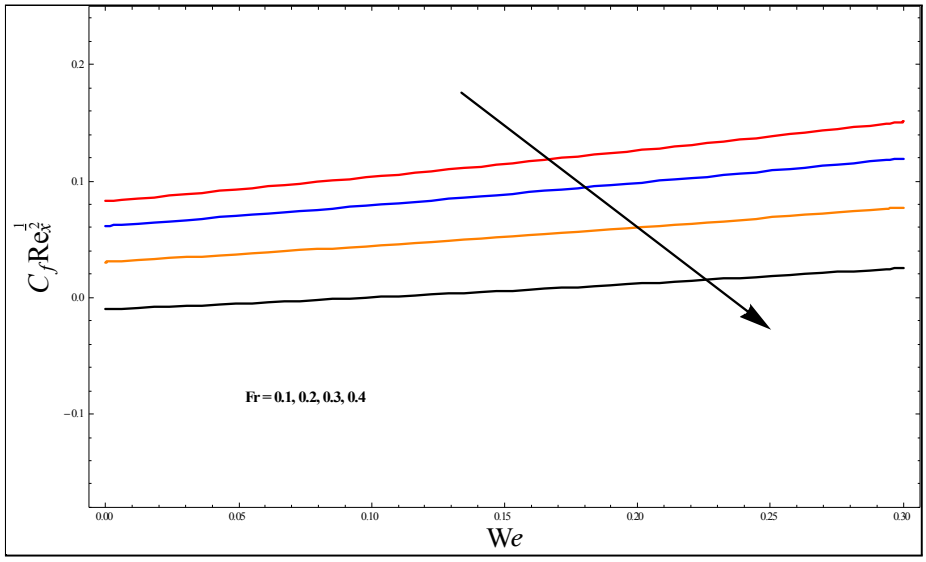

Fig. 3.19 Impact of Fr and We on Skin friction coeficient

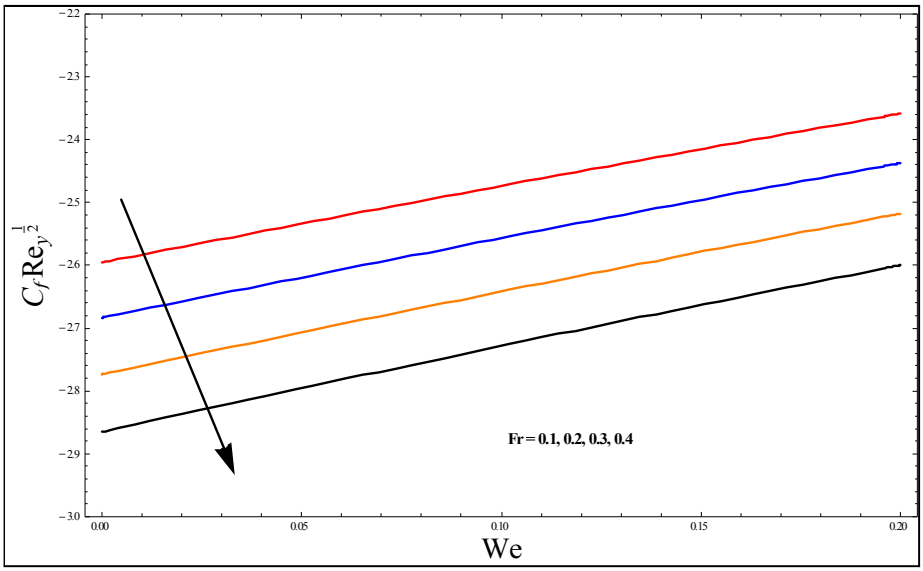

Fig. 3.20 Impact of Fr and We on Skin friction coeficient

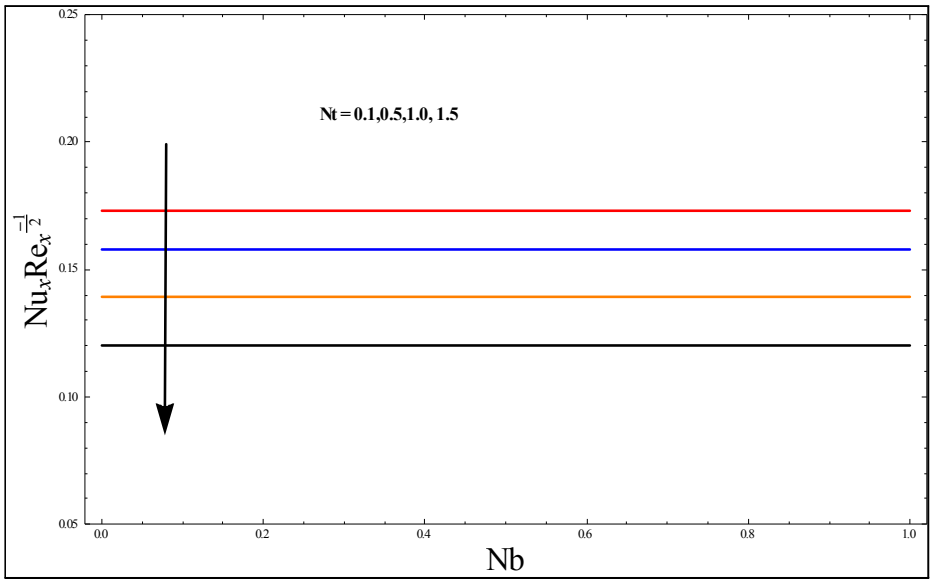

Fig. 3.21 Impact of Nt and Nb on Local Nusselt number

Chapter 4

Radiative 3D Powell Eyring Nano fluid Flow with Darcy-Forchheimer Effect past a nonlinear stretched surface

4.1 Mathematical modelling

In this chapter, we consider a 3D Powell Eyring nanofluid flow past a nonlinear stretched surface under the influence of nonlinear thermal radiation in a Darcy-Forchheimer porous media. The stretching is in the $x-$ and $y-$ directions with respective velocities $U_w(x,y) = a(x+y)^n$ and $V_w(x,y) = b(x+y)^n$ whereas $z-$ in the normal direction, with $a, b, n > 0$. At the boundary, convective heat and zero mass flux conditions are taken. The governing system representing the given scenario is given as:

$$u_x + v_y + w_z = 0, \tag{4.1}$$

$$uu_x + vu_y + wu_z = \left(\nu + \frac{1}{\rho_f \beta d_1}\right) u_{zz} - \frac{1}{2\beta d_1^3 \rho_f} (u_z)^2 u_{zz} - \frac{\nu}{k^*} u - Fu^2, \tag{4.2}$$

$$uv_x + vv_y + wv_z = \left(\nu + \frac{1}{\rho_f \beta d_1}\right) v_{zz} - \frac{1}{2\beta d_1^3 \rho_f} (v_z)^2 v_{zz} - \frac{\nu}{k^*} v - Fv^2, \tag{4.3}$$

$$uT_x + vT_y + wT_z = \alpha^* (T_{zz}) + \frac{(\rho c)_p}{(\rho c)_f} \left(D_B (T_z C_z) + \frac{D_T}{T_\infty} (T_z)^2\right) - \frac{1}{\rho C_p} (q_r)_z , \tag{4.4}$$

$$uC_x + vC_y + wC_z = D_B (C_{zz}) + \frac{D_T}{T_\infty} (T_{zz}) - k_c (C - C_\infty) . \tag{4.5}$$

supported by the boundary conditions

$$\begin{gathered} u = U_w,\ v = V_w,\ w = 0,\ -kT_z = h_f (T_f - T) , \\ D_B C_z + \frac{D_T}{T_\infty} T_z = 0 \text{ at } \ z = 0, \\ u \to 0, v \to 0,\ T \to T_\infty\ , C \to C_\infty \text{ as } z \to \infty. \end{gathered} \tag{4.6}$$

Dimensionless form of above mathematical model is obtained by utilizing following transformations:

$$\zeta = \sqrt{\left(\frac{a(n+1)}{2\nu}\right)} (x+y)^{\frac{(n-1)}{2}} z,\ \phi(\zeta) = \frac{C - C_\infty}{C_\infty},$$

$$\begin{aligned} u &= a (x+y)^n f'(\zeta) ,\ v = a (x+y)^n g'(\zeta) ,\ \theta(\zeta) = \frac{T - T_\infty}{T_f - T_\infty}, \\ w &= -\sqrt{\left(\frac{a\nu(n+1)}{2}\right)} (x+y)^{\frac{n-1}{2}} \left((f+g) + \left(\frac{n-1}{n+1}\right) \zeta \left(f' + g'\right)\right) . \end{aligned} \tag{4.7}$$

Here, satisfaction of Eq. (4.1) is inevitable. However, Eqs. $(4.2 - 4.6)$ take the form:

$$(1+\varepsilon) f''' + (f+g) f'' - \left(\frac{n+1}{2}\right) \varepsilon\delta f''^2 f'''' - \left(\frac{2\cdot n}{n+1}\right) \left(f' + g'\right) f' \tag{4.8}$$

$$- \left(\frac{2}{n+1}\right) \left(\lambda f' + Fr \left(f'\right)^2\right) = 0,$$

$$(1+\varepsilon) g''' + (f+g) g'' - \left(\frac{n+1}{2}\right) \varepsilon\delta g''^2 g'''' - \left(\frac{2\cdot n}{n+1}\right) \left(f' + g'\right) g' \tag{4.9}$$

$$-\left(\frac{2}{n+1}\right)\left(\lambda g'+Fr\left(g'\right)^2\right)=0,$$

$$\left(1+\frac{4}{3}Rd\left(1+\left(\theta_f-1\right)\theta\right)^3\right)\theta''+\Pr\left(\left(f+g\right)\theta'+Nb\theta'\phi'+Nt\theta'^2\right) \tag{4.10}$$

$$+\left(4Rd\left(1+\left(\theta_f-1\right)\theta\right)^2\left(\theta_f-1\right)\right)\theta'^2=0,$$

$$\phi''+Sc\left(f+g\right)\phi'+\frac{Nt}{Nb}\theta''-\frac{2}{n+1}Sc\delta_1\phi=0. \tag{4.11}$$

$$f(0)=0,\ g\left(0\right)=0,\ f'(0)=1,\ g'\left(0\right)=\alpha,\ \theta'\left(0\right)=-\gamma\left(1-\theta\left(0\right)\right),\ Nb\phi'\left(0\right)+Nt\theta'\left(0\right)=0,$$

$$f'(\infty)\to 0,\ g'\left(\infty\right)\to 0,\ \theta\left(\infty\right)\to 0,\ \phi(\infty)\to 0. \tag{4.12}$$

with

$$\varepsilon=\frac{1}{\rho_f\nu\beta d_1},\delta=\frac{a^3\left(x+y\right)^{3n-1}}{2\nu d_1^2},\lambda=\frac{\nu}{k^*a}\left(x+y\right)^{1-n},Rd=\frac{4\sigma^*{T_\infty}^3}{kk^*},Nt=\frac{\left(\rho c\right)_p D_T\left(T_f-T_\infty\right)}{\left(\rho c\right)_f\nu T_\infty},$$

$$\begin{aligned}\alpha &= \frac{b}{a},\theta_f=\frac{T_f}{T_\infty},\gamma=\frac{h}{k}\sqrt{\frac{\nu}{a}},\ Fr=\frac{C_b}{k^{*1/2}},\delta_1=\frac{k_c}{a}\left(x+y\right)^{1-n},\Pr=\frac{\nu}{\alpha^*},\\ Sc &= \frac{\nu}{D_B},\ Nb=\frac{\left(\rho c\right)_p D_B C_\infty}{\left(\rho c\right)_f\nu},Nt=\frac{\left(\rho c\right)_p D_T\left(T_f-T_\infty\right)}{\left(\rho c\right)_f\nu T_\infty}.\end{aligned} \tag{4.13}$$

The Nusselt number in dimensional form is given by:

$$Nu_x=\frac{\left(x+y\right)q_r}{k\left(T_f-T_\infty\right)}. \tag{4.14}$$

Dimensionless forms of the local Nusselt number is appended as follows:

$$Nu_x\,\mathrm{Re}_x^{\frac{-1}{2}}=-\left(\frac{n+1}{2}\right)^{\frac{1}{2}}\left(1+Rd\left[1+\left(\theta_f-1\right)\theta\left(0\right)\right]^3\right)\theta'\left(0\right). \tag{4.15}$$

In the existence of zero mass flux condition, the Sherwood number for zero mass flux condition is vanished and $\mathrm{Re}_x=\frac{U_w}{\nu}\left(x+y\right)$ expresses the local Reynolds number.

4.2 Homotopic solutions

The initial approximations $(f_0, g_0, \theta_0, \phi_0)$ and linear operators $(\mathrm{L}_f, \mathrm{L}_g, \mathrm{L}_\theta, \mathrm{L}_\phi)$ are selected as follows:

$$f_0(\zeta) = 1 - \exp(-\zeta), \qquad g_0(\zeta) = \alpha \cdot (1 - \exp(-\zeta)),$$

$$\theta_0(\zeta) = \left(\frac{\gamma}{\gamma+1}\right) \cdot (\exp(-\zeta), \qquad \phi_0(\zeta) = -\frac{\gamma}{\gamma+1}\left(\frac{N_t}{N_b}\right) \cdot \exp(-\zeta), \tag{4.16}$$

$$\mathrm{L}_f = f_{\zeta\zeta\zeta} - f_\zeta,\ \mathrm{L}_g = g_{\zeta\zeta\zeta} - g_\zeta,\ \mathrm{L}_\theta = \theta_{\zeta\zeta} - \theta,\ \mathrm{L}_\phi = \phi_{\zeta\zeta} - \phi, \tag{4.17}$$

with the properties

$$\mathrm{L}_f\ [q_1 + q_2 \exp(\zeta) + q_3 \exp(-\zeta)] = 0,$$

$$\mathrm{L}_g\ [q_4 + q_5 \exp(\zeta) + q_6 \exp(-\zeta)] = 0,$$

$$\mathrm{L}_\theta\ [q_7 \exp(\zeta) + q_8 \exp(-\zeta)] = 0,$$

$$\mathrm{L}_\phi\ [q_9 \exp(\zeta) + q_{10} \exp(-\zeta)] = 0, \tag{4.18}$$

where q_j and $[j = 1 - 10]$ are described as optional constants.

4.3 Convergence analysis

The parameters $\hbar_f, \hbar_g, \hbar_\theta$ and $\hbar_\phi$ have a vital role to decide the convergence of the homotopic solutions. The $\hbar$ curves are designed in fig 4.1. The allowable ranges of these parameters are are $-1.3 \leq \hbar_f \leq -0.4, -1.4 \leq \hbar_g \leq -0.3, -1.5 \leq \hbar_\theta \leq -0.5, -1.4 \leq \hbar_\phi \leq -0.4$. Table 4.1 is erected to see that 30th approximation is appropriate for these distributions. An excellent concurrence between the graphical and numerical results is witnessed.

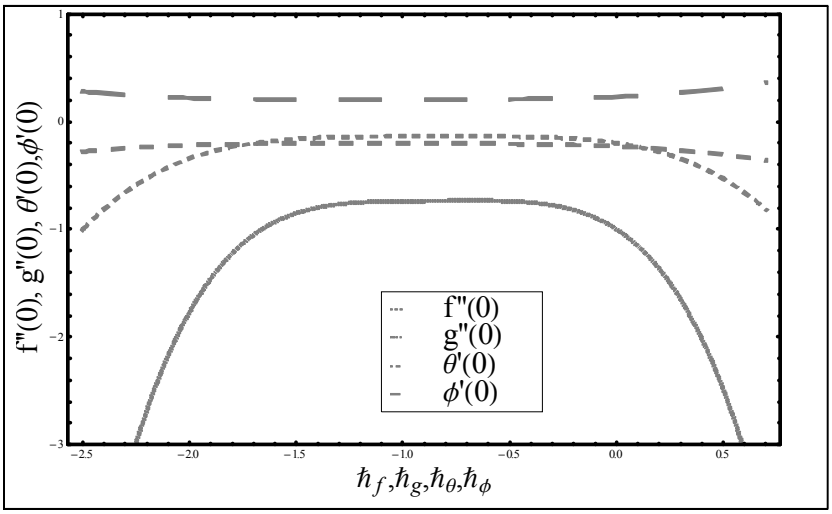

Fig 4.1 $\hbar-$ curves for f, g, θ and ϕ.

Table 4.1: Convergence of HAM solutions for different order of approximations

Order of approximations	$-f''(0)$	$-g''(0)$	$-\theta'(0)$	$\phi'(0)$
1	0.74256	0.14195	0.21402	0.07134
10	0.73190	0.13813	0.20821	0.06940
15	0.73358	0.13800	0.20564	0.06854
20	0.73593	0.13839	0.20445	0.06814
25	0.73590	0.13840	0.20447	0.06815
30	0.73590	0.13840	0.20447	0.06815

4.4 Results and discussions

This section is devoted to visualizing the impact of different physical parameters, on the velocities $f'(\zeta)$ and $g'(\zeta)$, temperature $\theta(\zeta)$ and concentration fields $\phi(\zeta)$. Figures 4.2 and 4.3 are sketched to see the influence of fluid parameters ε and δ on the velocity profile $f'(\zeta)$. It is witnessed that the velocity profile is an escalating and diminishing function of ε and δ respectively. Since $\varepsilon = \frac{1}{\rho_f \nu \beta d_1}$, so by increasing ε liquid's viscosity reduces, which ultimately enhanced the velocity. Also liquid become less viscous for greater values of ε. Whereas, by increasing δ, velocity reduces, this is due to the fact that viscosity of the liquid enhances by escalating values of δ. The impact of Forchheimer number on the velocity is displayed in figure 4.4. It is observed

that velocity $f'(\zeta)$ is lessening function of Fr. This is because, for the higher values of Fr lead to a resistance in a fluid flow. Figure 4.5 is drawn to show the trend of porosity number λ on the velocity distribution $f'(\zeta)$. It is experimented that the velocity of the fluid has dwindled for larger values of porosity parameter. Physically, the movement of the fluid is hindered due to the presence of porous media and this results in the falloff in the fluid's velocity. Figure 4.6 displays variation of Powell eyring parameter ε on the velocity field $g'(\zeta)$. Enhancement of velocity profile is observed for larger values of ε. Parameter ε is inversely proportional to the dynamic viscosity of the non newtonian liquid. So as ε increased, viscosity will reduced and velocity will enhanced. Figure 4.7 presents the effects of Powell eyring parameter δ on velocity field $g'(\zeta)$. An increment in δ, viscosity of the liquid enhanced that leads to lower velocity field. Figure 4.8 shows that greater Forchheimer number Fr results to lower velocity distribution $g'(\zeta)$. This is because, for the greater values of Fr lead to a resistance in a liquid flow. Figure 4.9 illustrates that the velocity distribution $g'(\zeta)$ is reduced for larger values of local porosity parameter λ. This is because, the movement of the liquid is hindered due to the presence of porous media, which produces resistance in the flow path and reduces the flow motion. To see the impact of Radiation parameter Rd on the temperature distribution $\theta(\zeta)$ is portrayed in figure 4.10. It is visualized that the temperature of the fluid augments for larger values of radiation parameter. Higher estimates of Rd obviously increase the temperature of the nanofluid as it is in direct proportionate to the nanofluid temperature at infinity. It can be seen from figure 4.11 that Prandtl number Pr clearly affects the process of heat transfer. Actually, is in inverse proportionate relation with the thermal diffusivity. Higher estimates of means a drop in thermal diffusivity of the nanofluid and as a decay in the fluid temperature is perceived. Figures 4.12 and 4.13 are portrayed to depict the influence of thermophoretic parameter Nt on the temperature $\theta(\zeta)$ and concentration $\phi(\zeta)$ fields. Actually, the smaller particles are pushed away from the hot surface towards the colder one. As a result, temperature and concentration of the fluid augments. To comprehend the relationship between the porosity number λ, the temperature ratio parameter θ_f and the temperature profile $\theta(\zeta)$, figures 4.14 and 4.15 are modeled. It is perceived that presence of permeable media offers hindrance to the movement of the fluid and ultimately increased temperature of the nanofluid is realized. Similar annotations are in case of θ_f. Figures 4.16 and 4.17 are portrayed to exhibit the effect of chemical reaction parameter

δ_1, for destructive case $\delta_1 > 0$, and generative case $\delta_1 < 0$, on concentration field $\phi(\zeta)$. An opposing trend in both cases is witnessed versus concentration profile. A slight decrement in the boundary layer thickness is observed in case of $\delta_1 > 0$ for gradually mounting values of δ_1. Enhancing values of δ_1 will repress the concentration of the liquid. Greater values of δ_1 would result in decrease of chemical molecular diffusivity, thus leading into reduction in diffusion. In figure 4.18, the image of Brownian motion parameter Nb against concentration field is depicted. For increasing estimates of Nb concentration is on decline. Actually, higher values of Nb trigger the random motion of tiny particles that results in high temperature and lower concentration. To visualize the result of Biot number γ versus concentration profile, figure 4.19 is drawn. As is linked with the heat transfer at the surface. Thus, an upsurge in γ, augments the thermal boundary layer and ultimately enhanced temperature is perceived. Figure 4.20 is formed to learn the behavior of Schmidt number Sc against the temperature field. For higher estimates of Sc feeble concentration is observed. In fact, Schmidt number is in inverse proportionate to Brownian diffusivity. Larger values of Sc results in lower Brownian diffusivity. This feeble Brownian diffusivity will lower the concentration profile. The characteristics of Nt and Sc on Nusselt number $Nu_x \operatorname{Re}_x^{\frac{-1}{2}}$ are displayed in figure 4.21. Interestingly $Nu_x \operatorname{Re}_x^{\frac{-1}{2}}$ increases for increasing values of Nt and Sc. Figure 4.22 illustrate the effect of Nt and δ_1 Nusselt number $Nu_x \operatorname{Re}_x^{\frac{-1}{2}}$. It is clear that $Nu_x \operatorname{Re}_x^{\frac{-1}{2}}$, reduces for larger values of Nt and δ_1.

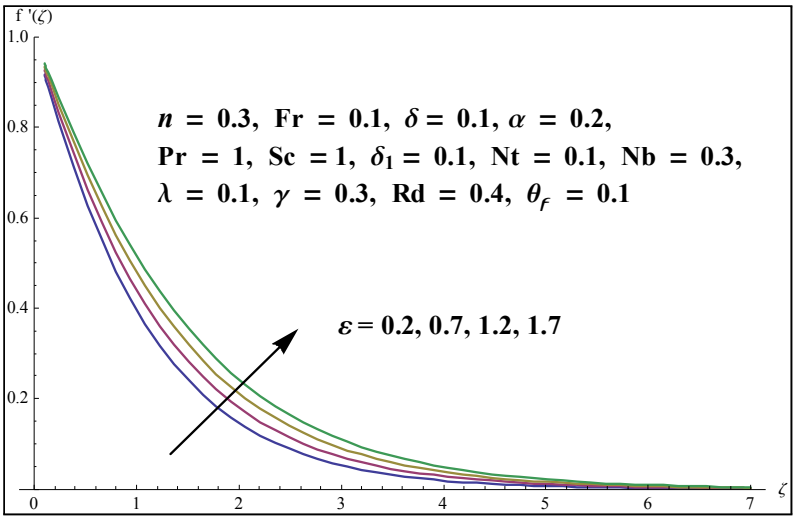

Fig. 4.2 Variation of ε on $f'(\zeta)$.

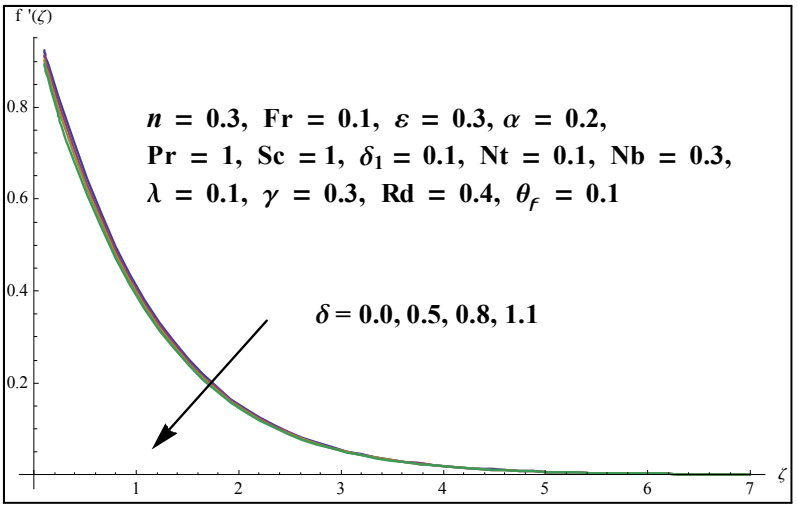

Fig. 4.3 Variation of δ on $f'(\zeta)$.

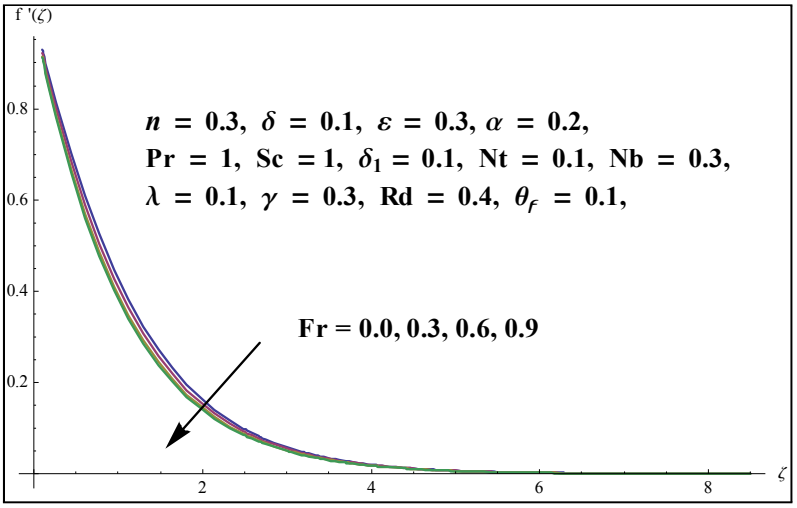

Fig. 4.4 Variation of Fr on $f'(\zeta)$.

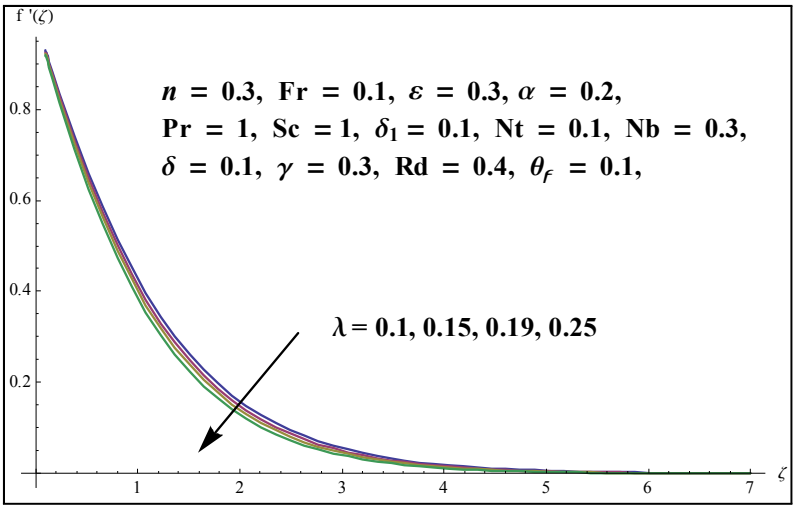

Fig. 4.5 Variation of λ on $f'(\zeta)$.

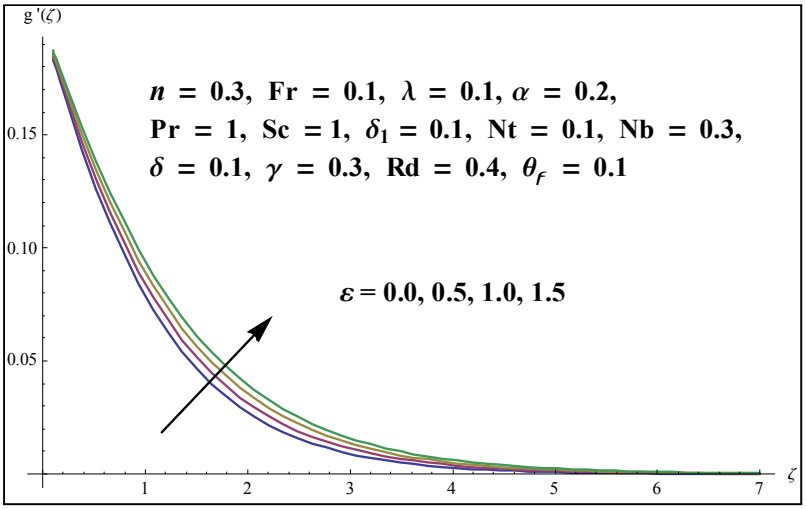

Fig. 4.6 Variation of ε on $g'(\zeta)$.

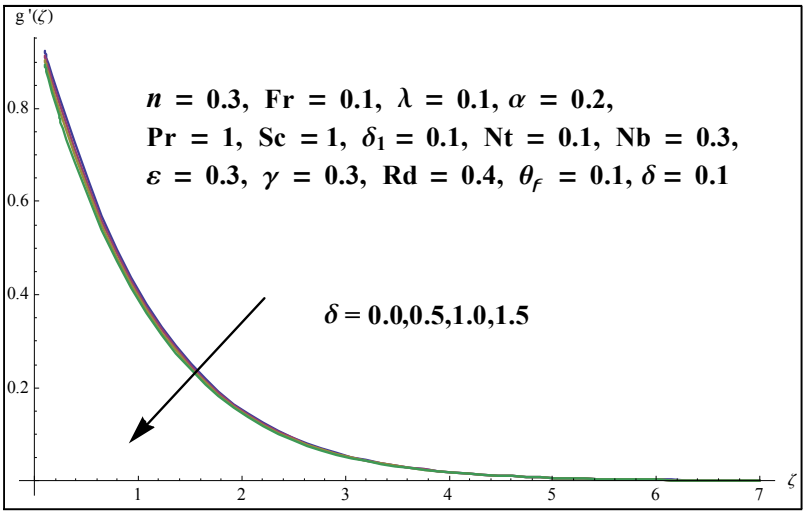

Fig. 4.7 Variation of δ on $g'(\zeta)$.

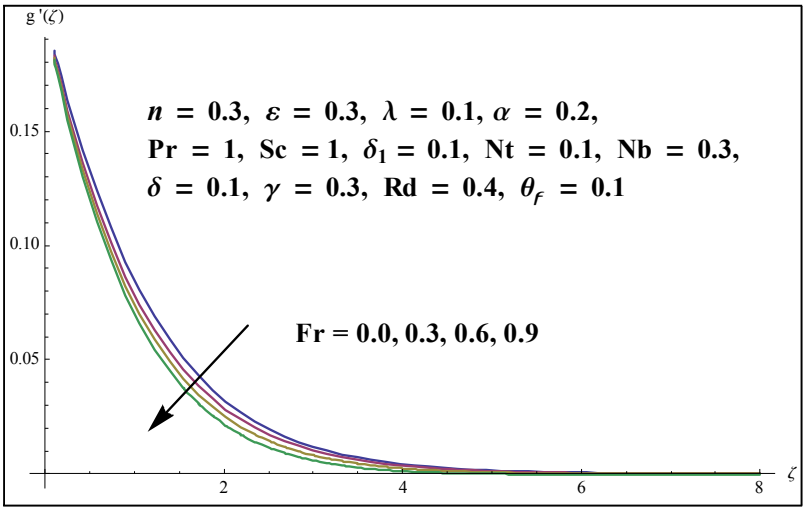

Fig. 4.8 Variation of Fr on $g'(\zeta)$.

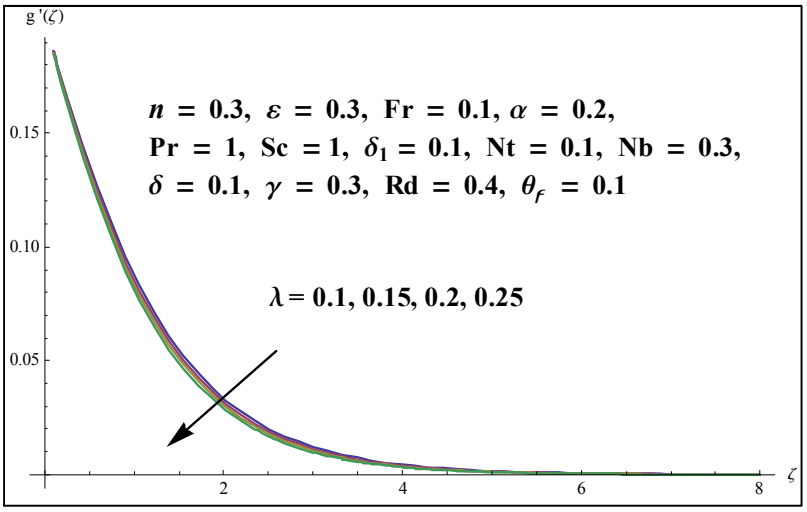

Fig. 4.9 Variation of λ on $g'(\zeta)$.

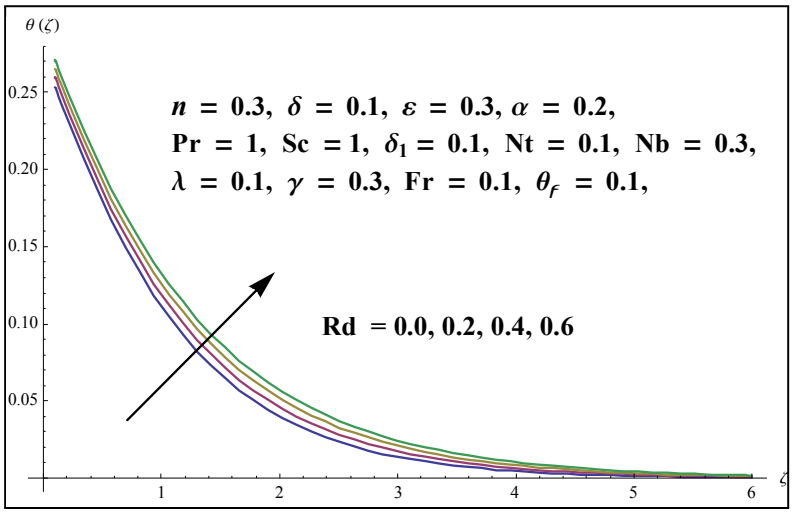

Fig. 4.10 Variation of Rd on $\theta(\zeta)$.

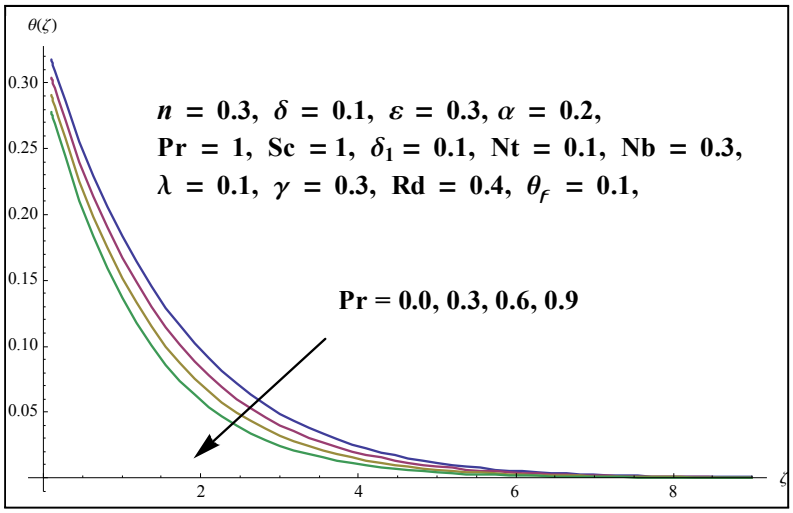

Fig. 4.11 Variation of Pr on $\theta(\zeta)$.

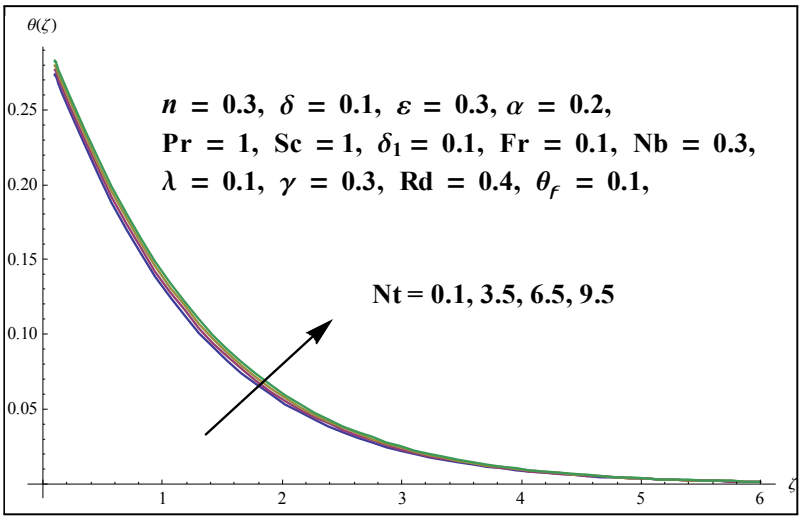

Fig. 4.12 Variation of Nt on $\theta(\zeta)$.

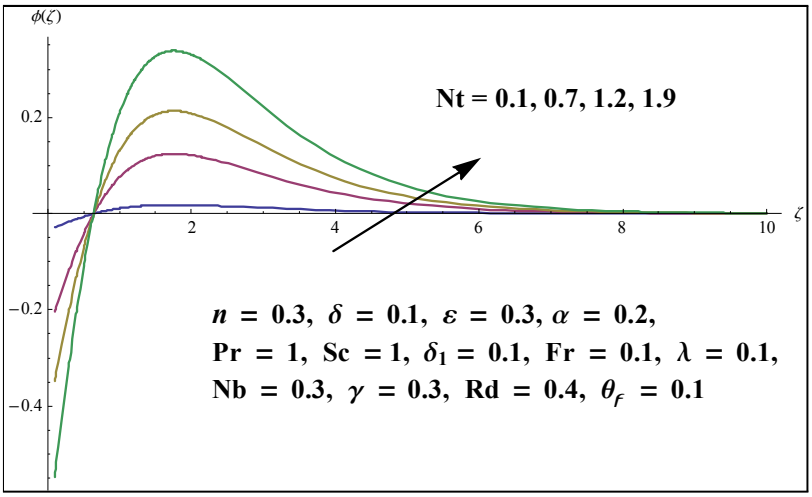

Fig. 4.13 Variation of Nt on $\phi(\zeta)$.

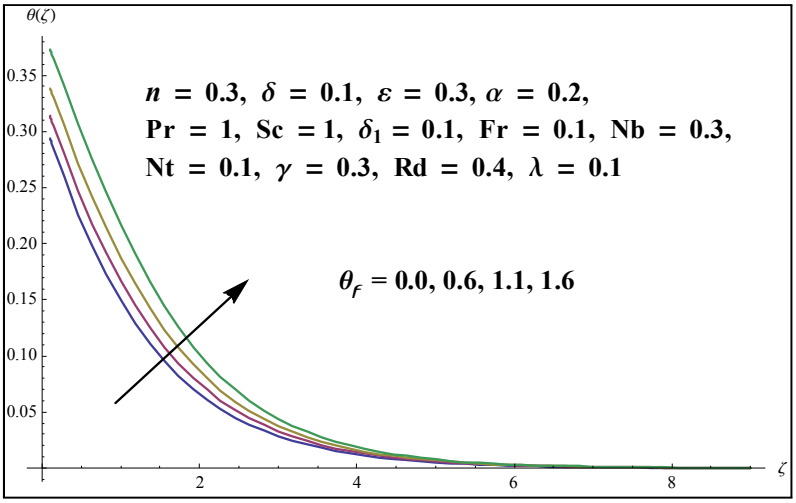

Fig. 4.14 Variation of θ_f on $\theta(\zeta)$.

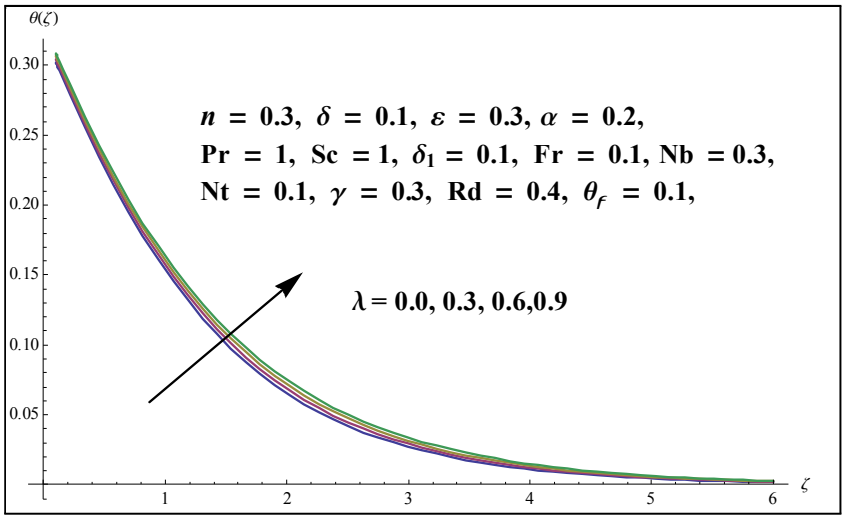

Fig. 4.15 Variation of λ on $\theta(\zeta)$.

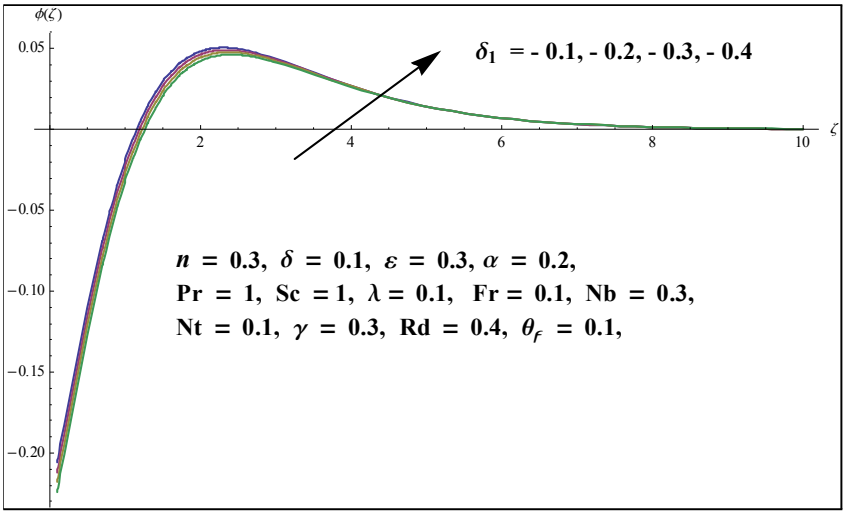

Fig. 4.16 Variation of $\delta_1 < 0$ on $\phi(\zeta)$.

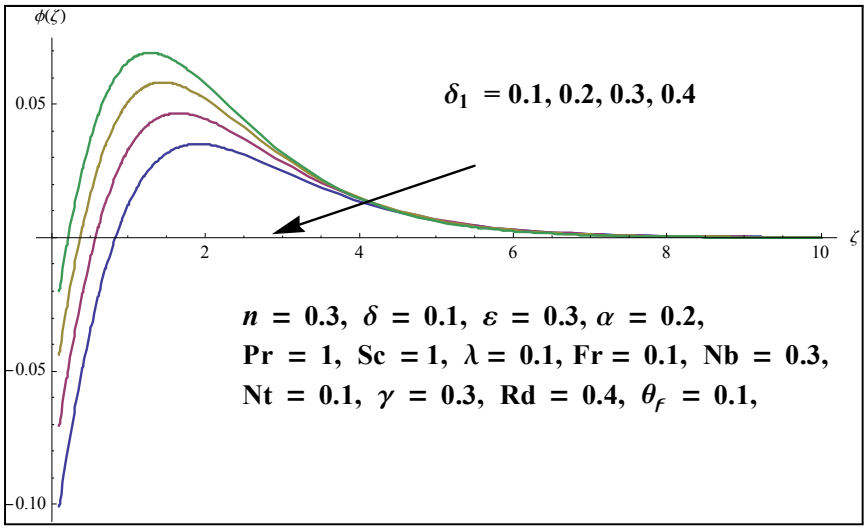

Fig. 4.17 Variation of $\delta_1 > 0$ on $\phi(\zeta)$.

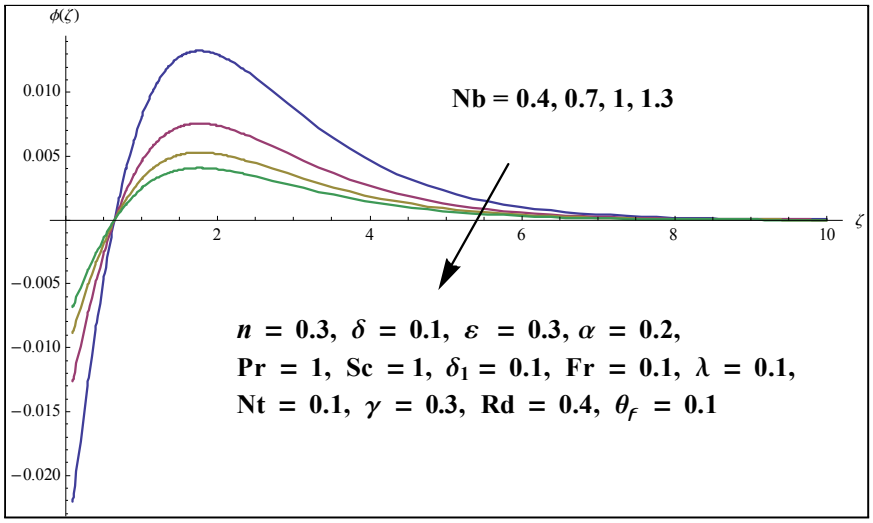

Fig. 4.18 Variation of Nb on $\phi(\zeta)$.

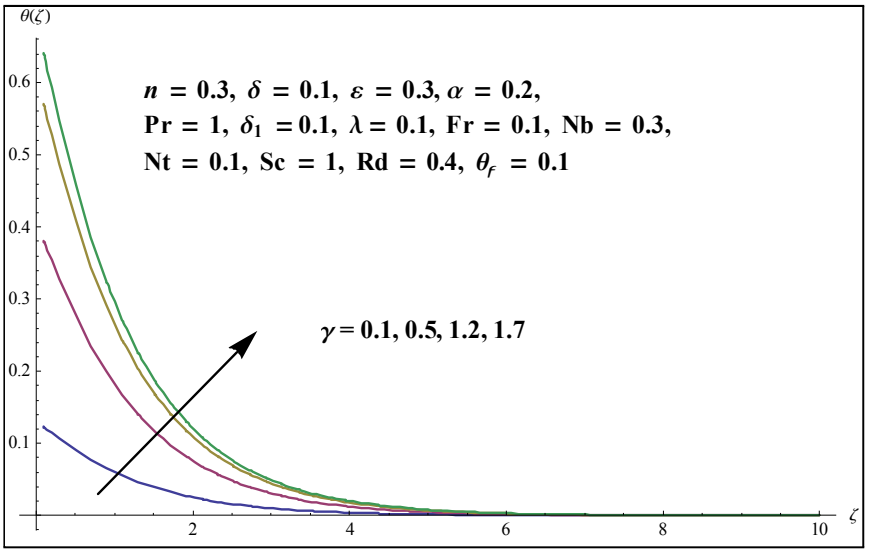

Fig. 4.19 Variation of γ on $\theta(\zeta)$.

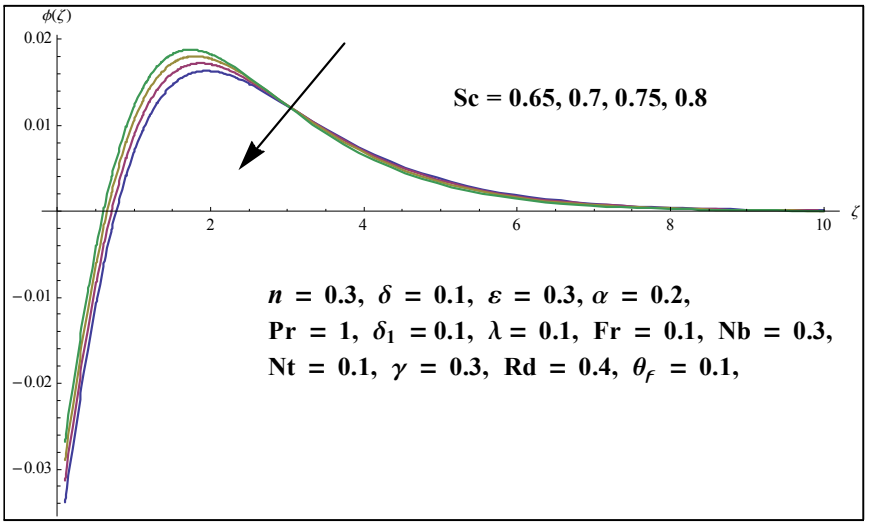

Fig. 4.20 Variation of Sc on $\theta(\zeta)$.

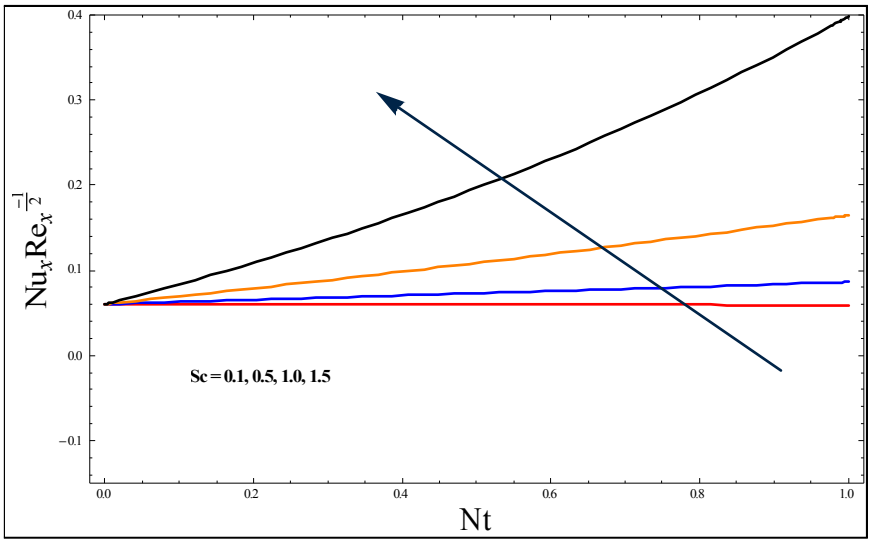

Fig. 4.21 Variation of Nt and Sc on Nusselt number.

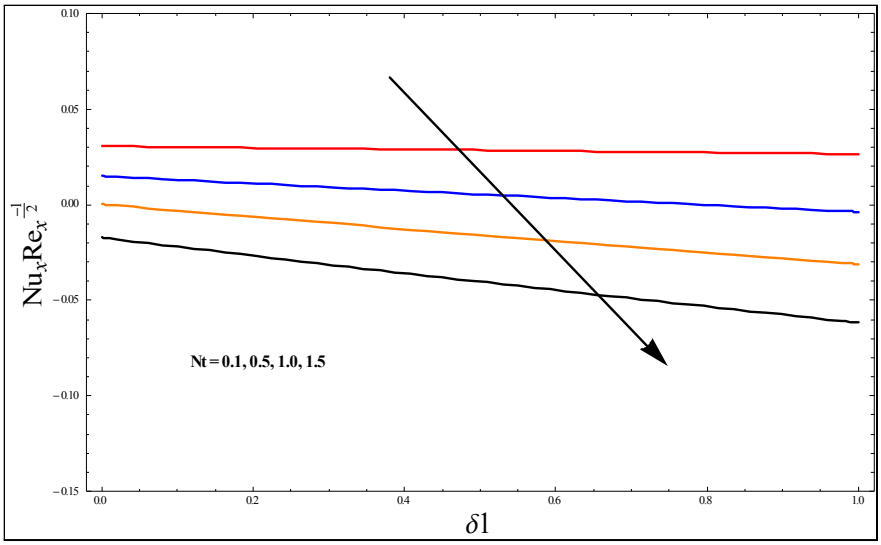

Fig. 4.22 Variation of Nt and δ_1 on Nusselt number.

Chapter 5

Conclusions and future work

In this thesis two problems have been analysed where first problem is about review paper and second problem is the extension work for it. Conclusion of both the problems are as following:

5.1 Chapter 3

In this section, we have studied the Darcy-Fochheimer 3D Williamson nanofluid flow over a convectively heated nonlinear strectching surface. Analytical solution of the problem is extracted by making use of renowned Homotopy Analysis method. The significant features of the problem are:

- The Thermophoresis parameter Nt enhances for both temperature and concentration distributions.
- Temperature profile increases for larger values of Forchheimer number Fr.
- For higher estimates of Biot number γ boosts in the temperature is observed.
- Concentration reduces for the escalating values of Brownian motion parameter Nb.
- Concentration decreases for higher values of Schmidt number.

5.2 Chapter 4

The present consideration is to analyze the steady 3D Eyring Powell nanofluid flow over a nonlinear stretchable surface with Darcy-Forchheimer spongy structure. Additional affects of chemical reaction with zero mass flux condition are also considered. The novelty of the presented model is enhanced by including the influence of nonlinear thermal radiation with convective boundary condition. Solution (analytical) of the problem is attained via HAM. The significant observations of the problem are appended as follows:

- The velocity profile is lessening function of Darcy-Forchheimer number Fr.
- For higher estimates of Schmidt number Sc feeble concentration is observed.
- The temperature of the fluid augments for escalating values of Radiation parameter Rd.
- For increasing estimates of Brownian motion Nb parameter concentration is on the decline.
- The velocity of the fluid has dwindled for larger values of porosity parameter λ.
- The Biot numbers γ increasing values augment the temperature of the fluid.

5.3 Future work

In this work, the effects of chemical reaction and nonlinear thermal radiaton on 3D Powell-Eyring nanofluid have been analyzed. However, there remains a need to further build on the current work so as to bring improvement about the concerned discourse. Few interesting possible extensions that could be researched in future are as follows:

- Any other non-Newtonian fluid along with appropriate boundary conditions.
- Bio-convective nanofluid with microorganisms.
- Boundary conditions also be changed to melting heat or second order slip.
- Flow over a curve surface with activation energy.

Bibliography

[1] Choi, S. U. S., & Eastman, J. A. (1995). Enhancing thermal conductivity of fluids with nanoparticles. ASME Int Mech Eng Congr Expo 66: 99–105.

[2] Saidur, R., Leong, K. Y., & Mohammad, H. (2011). A review on applications and challenges of nanofluids. Renewable and sustainable energy reviews, 15(3), 1646-1668.

[3] Wong, K. V., & De Leon, O. (2010). Applications of nanofluids: current and future. Advances in mechanical engineering, 2, 519659.

[4] Ramzan, M., Sheikholeslami, M., Saeed, M., & Chung, J. D. (2019). On the convective heat and zero nanoparticle mass flux conditions in the flow of 3D MHD Couple Stress nanofluid over an exponentially stretched surface. Scientific reports, 9(1), 562.

[5] Lu, D., Ramzan, M., Ahmad, S., Shafee, A., & Suleman, M. (2018). Impact of Nonlinear Thermal Radiation and Entropy Optimization Coatings with Hybrid Nanoliquid Flow Past a Curved Stretched Surface. Coatings, 8(12), 430.

[6] Muhammad, T., Lu, D. C., Mahanthesh, B., Eid, M. R., Ramzan, M., & Dar, A. (2018). Significance of Darcy-Forchheimer porous medium in nanofluid through carbon nanotubes. Communications in Theoretical Physics, 70(3), 361.

[7] Suleman, M., Ramzan, M., Zulfiqar, M., Bilal, M., Shafee, A., Chung, J. D., ... & Farooq, U. (2018). Entropy Analysis of 3D Non-Newtonian MHD Nanofluid Flow with Nonlinear Thermal Radiation Past over Exponential Stretched Surface. Entropy, 20(12), 930.

[8] Sheikholeslami, M., Shafee, A., Ramzan, M., & Li, Z. (2018). Investigation of Lorentz forces and radiation impacts on nanofluid treatment in a porous semi annulus via Darcy law. Journal of Molecular Liquids, 272, 8-14.

[9] Farooq, U., Lu, D., Ahmed, S., Ramzan, M., Chung, J. D., & Chandio, F. A. (2019). Computational Analysis for Mixed Convective Flows of Viscous Fluids With Nanoparticles. Journal of Thermal Science and Engineering Applications, 11(2), 021013.

[10] Ramzan, M., M. Sheikholeslami, Jae Dong Chung, and Ahmad Shafee. "Melting heat transfer and entropy optimization owing to carbon nanotubes suspended Casson nanoliquid flow past a swirling cylinder-A numerical treatment." AIP Advances 8, no. 11 (2018): 115130.

[11] Ramzan, M., Bilal, M., Chung, J. D., & Mann, A. B. (2018). On MHD radiative Jeffery nanofluid flow with convective heat and mass boundary conditions. Neural Computing and Applications, 30(9), 2739-2748.

[12] Lu, D., Ramzan, M., ul Huda, N., Chung, J. D., & Farooq, U. (2018). Nonlinear radiation effect on MHD Carreau nanofluid flow over a radially stretching surface with zero mass flux at the surface. Scientific reports, 8(1), 3709.

[13] Li, Z., Ramzan, M., Shafee, A., Saleem, S., Al-Mdallal, Q. M., & Chamkha, A. J. (2018). Numerical approach for nanofluid transportation due to electric force in a porous enclosure. Microsystem Technologies, 1-14.

[14] Lu, D., Ramzan, M., Ahmad, S., Chung, J. D., & Farooq, U. (2018). A numerical treatment of MHD radiative flow of Micropolar nanofluid with homogeneous-heterogeneous reactions past a nonlinear stretched surface. Scientific reports, 8(1), 12431.

[15] Lu, D. C., Ramzan, M., Bilal, M., Chung, J. D., & Farooq, U. (2018). Upshot of chemical species and nonlinear thermal radiation on Oldroyd-B nanofluid flow past a bi-directional stretched surface with heat generation/absorption in a porous media. Communications in Theoretical Physics, 70(1), 071.

[16] Darcy, H. (1856). Les fontaines publiques de la ville de Dijon: exposition et application... Victor Dalmont.

[17] Forchheimer, P. (1901). Wasserbewegung durch boden. Z. Ver. Deutsch, Ing., 45, 1782-1788.

[18] Muskat, M. (1946). The flow of homogeneous fluids through porous media (No. 532.5 M88).

[19] Pal, D., & Mondal, H. (2012). Hydromagnetic convective diffusion of species in Darcy–Forchheimer porous medium with non-uniform heat source/sink and variable viscosity. International Communications in Heat and Mass Transfer, 39(7), 913-917.

[20] Ganesh, N. V., Hakeem, A. A., & Ganga, B. (2016). Darcy–Forchheimer flow of hydromagnetic nanofluid over a stretching/shrinking sheet in a thermally stratified porous medium with second order slip, viscous and Ohmic dissipations effects. Ain Shams Engineering Journal, 9(4) 939-951.

[21] Alshomrani, A. S., & Ullah, M. Z. (2019). Effects of Homogeneous–Heterogeneous Reactions and Convective Condition in Darcy–Forchheimer Flow of Carbon Nanotubes. Journal of Heat Transfer, 141(1), 012405.

[22] Saif, R. S., Hayat, T., Ellahi, R., Muhammad, T., & Alsaedi, A. (2018). Darcy–Forchheimer flow of nanofluid due to a curved stretching surface. International Journal of Numerical Methods for Heat & Fluid Flow. DOI: 10.1108/HFF-08-2017-0301.

[23] Seth, G. S., Kumar, R., & Bhattacharyya, A. (2018). Entropy generation of dissipative flow of carbon nanotubes in rotating frame with Darcy-Forchheimer porous medium: A numerical study. Journal of Molecular Liquids, 268, 637-646.

[24] Hayat, T., Rafique, K., Muhammad, T., Alsaedi, A., & Ayub, M. (2018). Carbon nanotubes significance in Darcy-Forchheimer flow. Results in physics, 8, 26-33.

[25] Zeeshan, A., Maskeen, M. M., & Mehmood, O. U. (2018). Hydromagnetic nanofluid flow past a stretching cylinder embedded in non-Darcian Forchheimer porous media. Neural Computing and Applications, 30(11), 3479-3489.

[26] Tarakaramu, N., Narayana, P. S., & Venkateswarlu, B. (2019). MHD Three Dimensional Darcy-Forchheimer Flow of a Nanofluid with Nonlinear Thermal Radiation. In Applied Mathematics and Scientific Computing (pp. 87-97). Birkhäuser, Cham.

[27] RamReddy, C., Naveen, P., & Srinivasacharya, D. (2018). nonlinear convective flow of non-Newtonian fluid over an inclined plate with convective surface condition: a Darcy–Forchheimer model. International Journal of Applied and Computational Mathematics, 4(1), 51.

[28] Farooq, M., Ahmad, S., Javed, M., & Anjum, A. (2019). Melting heat transfer in squeezed nanofluid flow through Darcy Forchheimer medium. Journal of Heat Transfer, 141(1), 012402.

[29] Hayat, T., Ullah, I., Muhammad, T., Alsaedi, A., & Shehzad, S. A. (2016). Three-dimensional flow of Powell–Eyring nanofluid with heat and mass flux boundary conditions. Chinese Physics B, 25(7), 074701.

[30] Ramzan, M., Bilal, M., & Chung, J. D. (2017). Radiative flow of Powell-Eyring magneto-nanofluid over a stretching cylinder with chemical reaction and double stratification near a stagnation point. PloS one, 12(1), e0170790.

[31] Powell, R. E., & Eyring, H. (1944). Mechanisms for the relaxation theory of viscosity. Nature, 154(3909), 427.

[32] Patel, M., & Timol, M. G. (2009). Numerical treatment of Powell–Eyring fluid flow using method of satisfaction of asymptotic boundary conditions (MSABC). Applied Numerical Mathematics, 59(10), 2584-2592.

[33] Eldabe, N. T., Ghaly, A. Y., Mohamed, M. A., & Mahmoud, M. S. (2018). MHD boundary layer chemical reacting flow with heat transfer of Eyring–Powell nanofluid past a stretching sheet. Microsystem Technologies, 24(12), 4945-4953.

[34] Gholinia, M., Hosseinzadeh, K., Mehrzadi, H., Ganji, D. D., & Ranjbar, A. A. (2019). Investigation of MHD Eyring–Powell fluid flow over a rotating disk under effect of homogeneous–heterogeneous reactions. Case Studies in Thermal Engineering, 13, 100356.

[35] Upadhya, S. M., Raju, C. S. K., Shehzad, S. A., & Abbasi, F. M. (2018). Flow of Eyring-Powell dusty fluid in a deferment of aluminum and ferrous oxide nanoparticles with Cattaneo-Christov heat flux. Powder Technology, 340, 68-76.

[36] Ishaq, M., Ali, G., Shah, Z., Islam, S., & Muhammad, S. (2018). Entropy Generation on Nanofluid Thin Film Flow of Eyring–Powell Fluid with Thermal Radiation and MHD Effect on an Unsteady Porous Stretching Sheet. Entropy, 20(6), 412.

[37] Rauf, A., Abbas, Z., Shehzad, S. A., Alsaedi, A., & Hayat, T. (2018). Numerical simulation of chemically reactive Powell-Eyring liquid flow with double diffusive Cattaneo-Christov heat and mass flux theories. Applied Mathematics and Mechanics, 39(4), 467-476.

[38] Adesanya, S. O., Ogunseye, H. A., & Jangili, S. (2018). Unsteady squeezing flow of a radiative Eyring-Powell fluid channel flow with chemical reactions. International Journal of Thermal Sciences, 125, 440-447.

[39] Asha, S. K., & Sunitha, G. (2019). Effect of joule heating and MHD on peristaltic blood flow of Eyring–Powell nanofluid in a non-uniform channel. Journal of Taibah University for Science, 13(1), 155-168.

[40] Alharbi, S., Dawar, A., Shah, Z., Khan, W., Idrees, M., Islam, S., & Khan, I. (2018). Entropy Generation in MHD Eyring–Powell Fluid Flow over an Unsteady Oscillatory Porous Stretching Surface under the Impact of Thermal Radiation and Heat Source/Sink. Applied Sciences, 8(12), 2588.

[41] Ramzan, M., Bilal, M., Chung, J. D., Lu, D. C., & Farooq, U. (2017). Impact of generalized Fourier's and Fick's laws on MHD 3D second grade nanofluid flow with variable thermal conductivity and convective heat and mass conditions. Physics of Fluids, 29(9), 093102.

[42] Ramzan, M., Bilal, M., Kanwal, S., & Chung, J. D. (2017). Effects of variable thermal conductivity and non-linear thermal radiation past an Eyring Powell nanofluid flow with chemical Reaction. Communications in Theoretical Physics, 67(6), 723.

[43] Ramzan, M., Bilal, M., & Chung, J. D. (2017). Influence of homogeneous-heterogeneous reactions on MHD 3D Maxwell fluid flow with Cattaneo-Christov heat flux and convective boundary condition. Journal of Molecular Liquids, 230, 415-422.

[44] Ramzan, M., Bilal, M., Chung, J. D., & Mann, A. B. (2018). On MHD radiative Jeffery nanofluid flow with convective heat and mass boundary conditions. Neural Computing and Applications, 30(9), 2739-2748.

Radiative 3D Powell Eyring Nanofluid flow with Darcy-Forchheimer effect past a nonlinear strectched surface

ORIGINALITY REPORT

14%	3%	8%	13%
SIMILARITY INDEX	INTERNET SOURCES	PUBLICATIONS	STUDENT PAPERS

PRIMARY SOURCES

1	Submitted to Higher Education Commission Pakistan Student Paper	8%
2	Tasawar Hayat, Arsalan Aziz, Taseer Muhammad, Ahmed Alsaedi. "Darcy–Forchheimer Three-Dimensional Flow of Williamson Nanofluid over a Convectively Heated Nonlinear Stretching Surface", Communications in Theoretical Physics, 2017 Publication	1%
3	aip.scitation.org Internet Source	<1%
4	Submitted to Institute Vinca Student Paper	<1%
5	Dian-Chen Lu, M. Ramzan, M. Bilal, Jae Dong Chung, Umer Farooq. "Upshot of Chemical Species and Nonlinear Thermal Radiation on Oldroyd-B Nanofluid Flow Past a Bi-directional Stretched Surface with Heat	<1%